PHYSICAL REVIEW A VOLUME 46, NUMBER 11 1 DECEMBER 1992

Probe transmission in one-dimensional optical molasses: Theory for linearly cross-polarized cooling beams

J.-Y. Courtois and G. Grynberg
Laboratoire de Spectroscopie Hertzienne de l'Ecole Normale Supérieure, Université Pierre et Marie Curie, Case 74, T12-E01, F-75252 Paris CEDEX 05, France
(Received 15 June 1992)

We present a detailed theoretical investigation of the transmission spectrum of a probe beam interacting with atoms in a one-dimensional optical molasses obtained with linearly cross-polarized counterpropagating pump beams. The study is performed for a $J_g=\frac{1}{2}\rightarrow J_e=\frac{3}{2}$ atomic transition in the limit where the Hamiltonian part of the atom-field coupling is predominant over the relaxation part. We analyze the stimulated Raman transitions occurring between different vibrational levels of the atoms in the periodic potential created by the light shifts, and we show a dramatic lengthening of the damping time of coherences between such levels due to the Lamb-Dicke effect. Very narrow Rayleigh resonances with a shape sensitive to the probe polarization appear for a probe frequency close to the pump frequency. We interpret these resonances in terms of scattering of the pump waves on density and magnetization gratings, and show that they provide important information about the dynamics and localization of atoms at the bottom of the potential wells. Such information should also be accessed by phase-conjugation experiments. Finally, indications on the treatment of other atomic transitions are given.

PACS number(s): 32.80.Pj, 32.70.Jz, 42.65.−k

INTRODUCTION

It is well known from both a theoretical and an experimental point of view that the potential wells created by the light shift may be used to trap atoms. Theoretically, Castin and Dalibard [1] have predicted that in the case where two counterpropagating cooling beams have orthogonal linear polarizations (lin⊥lin polarization) the light shifts experienced by the atomic Zeeman sublevels lead to a periodic potential which gives rise to atom localization on the wavelength scale and to an energy-band structure for the atoms. Experimentally, Westbrook *et al.* have demonstrated the existence of localization in three-dimensional (3D) optical molasses by observing a Dicke narrowing of the fluorescence [2]. More recently, Verkerk *et al.* [3] have studied the probe absorption by a 1D cesium optical molasses made from two counterpropagating linearly cross-polarized beams. They have observed narrow resonances which can be attributed on one hand to Raman transitions between different bands and on the other hand to Rayleigh resonances which provide information about the localization and the dynamics of atoms in the potential wells. One particularly important and surprising feature of these resonances is that their widths are more than one order of magnitude smaller than the optical pumping rate. The aim of this article is to give a detailed description of the position and the shape of the resonances that can be observed on the probe transmission and on the probe phase-conjugate reflection. Our theoretical investigation is based on the band model of [1] and is performed for a $J_g=\frac{1}{2}\rightarrow J_e=\frac{3}{2}$ atomic transition. In Sec. I we first recall the most important features of atoms interacting with two lin⊥lin pump beams (geometry of Sisyphus cooling) which are essential to understand this paper. We then give a qualitative interpretation of the characteristic evolution times (associated with the width of the resonances) for two limiting cases. We first show that in the limit of strong atom localization a dramatic lengthening of effective lifetimes for some atomic variables occurs because of the Lamb-Dicke effect. Another effect involving highly excited states for the external degrees of freedom takes place in the limit of weak atom localization and leads also to very long damping times foı some atomic variables. These effects are at the origin of the very narrow widths observed in the experiment. In Sec. II we turn to a more rigorous analysis and we discuss in detail all the important features of the resonances. We finally give some ideas about the treatment of this problem in the case of other atomic transitions.

Our aim here is to extend the formalism of [1] to the case of pump-probe experiments. Our theoretical description is to first order in the amplitude of the probe field. We are thus in a situation where the linear-response theory can be applied [4]. In such a situation, the probe excites some particular evolution modes of the atom in the 1D optical molasses but does not modify its dynamical characteristics. For example, the widths of the resonances obtained in pump-probe experiments only depend on the dynamics of the atoms in the 1D optical molasses in absence of probe. The various shapes of the transmission spectra obtained for different polarization configurations of the probe arise from the different dynamical evolution modes of an atom in a 1D optical molasses that are excited by the probe in each polarization configuration.

By comparison with earlier theoretical descriptions of pump-probe interaction in cold atomic vapors [5], we do not assume a particular form for the momentum distribution (this could be achieved through the interaction with a reservoir at temperature T). In contrast, the population distribution in the different Hamiltonian eigenstates arises from the interaction of the atom with the incident fields and is thus a dynamical variable in our approach. Also the choice of molasses polarizations that we study here puts the emphasis on the bound states of the atoms in the optical potential wells while the recoil-induced resonances of [5] are actually associated with Raman transitions between continuum states.

I. ATOMS IN THE PRESENCE OF THE PUMP BEAMS

A. Presentation of the model

We consider the simple case of a 1D optical molasses in the geometry of Sisyphus cooling for an atomic transition between a $J_g=\frac{1}{2}$ ground state and a $J_e=\frac{3}{2}$ excited state [6–8]. The cooling field results from the superposition of two counterpropagating pump waves of wavelength $\lambda=2\pi/k$, traveling along the $+z$ and $-z$ directions. These waves have the same frequency ω, the same amplitude E_0, and are polarized along Ox and Oy, respectively. The resulting polarization of light exhibits a spatially periodic gradient of ellipticity: for a convenient choice of phases, it is circularly polarized σ^- at $z=0$, linear at $z=\lambda/8$, circularly polarized σ^+ at $z=\lambda/4$, linear at $z=3\lambda/8, \ldots$ (Fig. 1).

The effect of the interaction between an atom and this field can be split into two parts [9].

(i) On one hand, the reactive part associated with light shifts results in a sinusoidal periodic potential $U_\pm^{(0)}(z)$ depending on the atomic ground-state sublevel $|g,\pm\rangle$ [1]

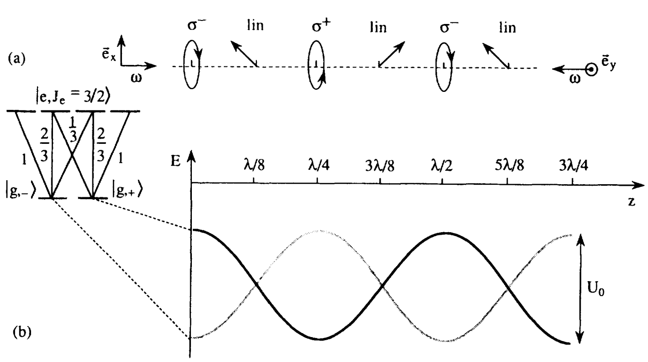

FIG. 1. Polarization gradient in a lin⊥lin 1D optical molasses and associated light-shifted Zeeman sublevels for a $J_g=\frac{1}{2}\rightarrow J_e=\frac{3}{2}$ atomic transition. (a) The cooling wave results from the superposition of two linearly cross-polarized counterpropagating beams having the same intensity and wavelength λ. The resulting polarization exhibits a space-dependent ellipticity. For a convenient choice of phase of the cooling beams, it is σ^- for $z=0$, linear along $(\mathbf{e}_x-\mathbf{e}_y)/\sqrt{2}$ for $z=\lambda/8$, σ^+ for $z=\lambda/4$, linear along $(\mathbf{e}_x+\mathbf{e}_y)/\sqrt{2}$ for $z=3\lambda/8$. (b) The spatial modulation of ellipticity results into a spatially periodic (period $\lambda/2$) modulation of the energies of the light-shifted ground-state Zeeman sublevels.

(Fig. 1):

$$U_\pm^{(0)}(z)=\frac{U_0}{2}[-2\pm\cos(2kz)] , \tag{1}$$

with

$$U_0=-\frac{2}{3}\hbar\Delta s_0 \tag{2}$$

and

$$s_0=\frac{\Omega^2/2}{\Delta^2+\Gamma^2/4} , \tag{3}$$

where $\Omega=-2dE_0/\hbar$ is the resonant Rabi frequency which characterizes the coupling between the atomic dipole d and the field, Γ is the natural width of the atomic excited state, and $\Delta=\omega-\omega_A$ is the detuning between the pump beams (ω) and the atomic (ω_A) frequency (we assume $\Delta<0$, atomic cooling occurring on the red side of the resonance). This reactive contribution may be characterized by the oscillation frequency Ω_v of the atoms at the bottom of a potential well $U_\pm^{(0)}(z)$. For example, near $z=0$ the potential $U_-^{(0)}(z)$ can be approximated by $U_-^{(h)}(z)$ with

$$U_-^{(h)}(z)=-\tfrac{3}{2}U_0+U_0k^2z^2 \tag{4}$$

and the characteristic oscillation frequency Ω_v is given by

$$\Omega_v=\frac{2U_0}{\hbar}\sqrt{E_R/U_0} , \tag{5}$$

where $E_R=\hbar^2k^2/2M$ is the atomic recoil energy, M being the atomic mass.

(ii) On the other hand, the dissipative part of the atom-field interaction accounts for processes where absorption of a laser photon is followed by spontaneous emission. These processes are in particular responsible for real transitions between $|g,+\rangle$ and $|g,-\rangle$ (optical pumping) which give rise to finite lifetimes of the ground-state sublevels and interrupt the oscillating motion of the atoms in the potential. This contribution is characterized by the optical pumping rate $\gamma_0=\frac{2}{9}\Gamma s_0$. It should be noticed that γ_0 characterizes the transfer rate between the two Zeeman sublevels. If one wishes to calculate at which rate an atom scatters radiation from the incident field, one should rather use

$$\Gamma'=\Gamma s_0 . \tag{6}$$

The difference between Γ' and γ_0 arises from the fact that an atom can return to its *initial* sublevel through an absorption-spontaneous emission cycle, the multiplicative factor $\frac{2}{9}$ between γ_0 and Γ' ($\gamma_0=\frac{2}{9}\Gamma'$) being associated with the particular Clebsch-Gordan coefficients of the $J_g=\frac{1}{2}\rightarrow J_e=\frac{3}{2}$ transition.

Since we want to describe the properties of localized cold atoms, we restrict ourselves to the regime where the reactive part of the atom-field coupling is predominant over the dissipative part

$$\Omega_v \gg \Gamma' \tag{7}$$

and to the low saturation domain

$$s_0 \ll 1 \, , \tag{8}$$

which have been proved to lead to the lowest temperatures [10]. Condition (8) indicates that atoms remain mainly in the internal ground-state sublevels. Condition (7) means classically that an atom oscillates many times at the bottom of the potential before its oscillating motion is interrupted by an absorption-spontaneous emission cycle. For a given depth of the potential U_0, this condition is fulfilled in the limit of large detunings Δ.

In this regime, all the physical phenomena can be interpreted by means of the eigenstates of the Hamiltonian $H^{(0)}$ associated with the potential $U_{\pm}^{(0)}(z)$:

$$H^{(0)} = \frac{P^2}{2M} + U_{-}^{(0)}(Z)|g,-\rangle\langle g,-| + U_{+}^{(0)}(Z)|g,+\rangle\langle g,+| \, , \tag{9}$$

where P and Z are the momentum and position operators of the atomic center of mass. This Hamiltonian contains the atomic kinetic energy and the reactive part of the atom-field coupling and is completely characterized by only one dimensionless parameter U_0/E_R. Due to the periodicity ($\lambda/2$) of the potential, the energy spectrum of the atoms displays a band structure similar to the one of electrons in a crystal. Following the Bloch theorem [11], the associated eigenstates can be labeled as $|n,q,\mu\rangle$ where n is a positive integer labeling the band, and where $\mu = \pm$ stands for the internal state $|g,\pm\rangle$. q is the Bloch index which lies within the first Brillouin zone ($-k < q \leq k$) and takes only discrete values when periodic boundary conditions in a box of finite size (an integer number of the potential period $\lambda/2$) are used.

As will be shown in Sec. II, wave functions $|n,q,\mu\rangle$ are very convenient for numerical calculations. However, these completely delocalized eigenstates are not suited to describe atoms of band n localized near the bottom of a given potential well. This situation, well known in the tight binding approximation for electrons in a crystal, can be described by a linear combination of the Bloch functions $|n,q\rangle$ of band n (Wannier function). For sufficiently deep potential wells and for small values of n, the Wannier function roughly corresponds to an eigenstate of the Hamiltonian of an atom in a single well-defined potential well. Such a state should have a spatial extension Δz very small compared to $\lambda/2$. It then corresponds to the intuitive representation of an atom well localized at the bottom of a potential well. In this regime, called Lamb-Dicke regime, the potential $U_{-}^{(0)}(z)$ can be approximated near $z=0$ by the harmonic potential given in (4). The Wannier function and the energy of the lowest bands are then approximated by the corresponding wave function and energy of the harmonic oscillator of angular frequency Ω_v. Because the extension Δz of the harmonic oscillator wave function scales as $\sqrt{\hbar/M\Omega_v}$, the small parameter characterizing the Lamb-Dicke regime is

$$k\,\Delta z \approx \left[\frac{E_R}{U_0}\right]^{1/4} \approx \left[\frac{E_R}{\hbar\Omega_v}\right]^{1/2} \ll 1 \, . \tag{10}$$

The use of Wannier functions instead of Bloch functions is certainly appropriate when the tunneling rate from one well to another is much smaller than the effective lifetime of an atom in a given state caused by absorption-spontaneous emission processes.

As will be shown in the following, a localized atom in a bound vibrational level of the optical potential presents some typical characteristics in the Lamb-Dicke regime when (7) and (8) are fulfilled. The pump-probe transmission spectra reported in [3] display ultranarrow resonances which demonstrate the occurrence of damping rates much smaller than the typical optical pumping rate Γ'. This result is very surprising since one would expect both the populations of the vibrational states and the coherences between different bands to decay with a rate similar to the absorption-spontaneous emission cycles which occur at the rate Γ'. In order to understand the origin of these narrow resonances, we first aim at giving a qualitative interpretation of the typical damping rates of some atomic variables. We distinguish two limiting cases of strong and weak atom localization and we show that a dramatic lengthening of the atomic lifetimes can occur in both situations.

B. Influence of localization on damping rates of populations and coherences: The Lamb-Dicke effect

We show here that in the case of sufficiently deep potential wells, localization of atoms at the bottom of the potential wells is responsible for a spectacular lengthening of the relaxation time of populations and coherences. Let us consider a bound state having an atomic wave function well localized near the bottom of the potential $U_{-}^{(0)}$ where the resulting trapping wave is σ^- polarized and the internal atomic state is $|g,-\rangle$. At this location, the prevailing process undergone by the atom is absorption from the Zeeman sublevel $|g,-\rangle$ to $|e,-\frac{3}{2}\rangle$ from where it can only return to $|g,-\rangle$ (because the Clebsch-Gordan coefficient of the transition is equal to 1). The probability of escaping from $U_{-}^{(0)}$ to a band of $U_{+}^{(0)}$ is small because the transition probability of going from $U_{-}^{(0)}$ to $U_{+}^{(0)}$ depends on the amount of the σ^+ component over the spatial extension of the atomic wave function, which is here very small. Furthermore, the probability of reaching another vibrational band of the potential $U_{-}^{(0)}$ is reduced by the Lamb-Dicke effect, similarly to the case of trapped ions [12]. More precisely, the transfer of momentum ($\approx \hbar k$) in the scattering process is small compared to the width in momentum space of the initial vibrational wave function ($\approx \sqrt{\hbar M \Omega_v}$) because $E_R \ll \hbar\Omega_v$ [see Eq. (10)]. The atomic state at the end of the scattering process has then a very small overlap with the other vibrational wave functions and has a probability close to 1 to coincide with the initial wave function. The damping rate of the populations of the lowest bands is thus considerably reduced because *several absorption-spontaneous emission cycles are needed to induce a transfer onto other levels.* Similarly, coherences between two vibrational states at the bottom of the potential well are only destroyed after several absorption-spontaneous emission cycles.

In the Lamb-Dicke regime where the wave functions of the lowest bands can be approximated by those of an harmonic oscillator, it is possible to estimate the order of magnitude of these damping rates. We first consider the transition rate from $|g,-\rangle\otimes|\phi_n\rangle$ [where $|\phi_n\rangle$ is the eigenstate of the harmonic oscillator located around $z=0$ and having energy $(n+\frac{1}{2})\hbar\Omega_v$] to any $|g,+\rangle$ state. Because the light polarization $\mathbf{e}_0$ of the pump at a point z is [8]:

$$\mathbf{e}_0=\cos(kz)\mathbf{e}_- - i\sin(kz)\mathbf{e}_+ \tag{11}$$

(where $\mathbf{e}_-$ and $\mathbf{e}_+$ respectively correspond to the σ^- and σ^+ circular polarizations), the average transfer rate from $|g,-\rangle\otimes|\phi_n\rangle$ to the $|g,+\rangle$ states is

$$\Gamma_n^{(1)}=\gamma_0\langle\phi_n|\sin^2(kZ)|\phi_n\rangle , \tag{12}$$

which involves the average of the σ^+ component of the light over the atomic wave function. For the lowest bound states, we can use $\sin^2(kZ)\approx k^2Z^2$ which, using the well-known value of $\langle\phi_n|k^2Z^2|\phi_n\rangle$ for a harmonic oscillator $[\langle\phi_n|k^2Z^2|\phi_n\rangle=(n+\frac{1}{2})\hbar k^2/M\Omega_v]$, yields

$$\Gamma_n^{(1)}=\gamma_0\left[n+\frac{1}{2}\right]\sqrt{E_R/U_0} . \tag{13}$$

We now consider the transition rate from $|g,-\rangle\otimes|\phi_n\rangle$ to another state $|g,-\rangle\otimes|\phi_m\rangle$ of the same potential well. This transition may be written as

$$\Gamma_{n\to m}=\Gamma'[\,\overline{|\langle\phi_n|\cos(kZ)e^{ipZ}|\phi_m\rangle|^2} + \overline{|\tfrac{1}{3}\langle\phi_n|\sin(kZ)e^{ipZ}|\phi_m\rangle|^2}\,] , \tag{14}$$

where p is the component of the wave vector of the spontaneous emitted photon along the z axis and the symbol $\overline{(\ )}$ describes the average over the direction of emission of the photon. The first term of the right-hand side of (14) corresponds to the absorption of a σ^- photon followed by the emission of a σ^- photon and the second term to a process where two σ^+ photons are involved. The factor $\frac{1}{3}$ in the second term is the square of the Clebsch-Gordan coefficient coupling $|g,-\rangle$ to $|e,+\frac{1}{2}\rangle$.

The transfer rate to any level $n\neq m$ is readily obtained by summing (14) and using the closure relation

$$\Gamma_n^{(2)}=\Gamma'[\,\langle\phi_n|\cos^2(kZ)+\tfrac{1}{9}\sin^2(kZ)|\phi_n\rangle - \overline{|\langle\phi_n|\cos(kZ)e^{ipZ}|\phi_n\rangle|^2} - \overline{|\tfrac{1}{3}\langle\phi_n|\sin(kZ)e^{ipZ}|\phi_n\rangle|^2}\,] . \tag{15}$$

To obtain a rough estimate of $\Gamma_n^{(2)}$, we simply assume in this section that the photons are emitted along the z axis (with an equal probability in the $+z$ and $-z$ directions). Expanding $\cos(kZ)$, $\sin(kZ)$, and e^{ikZ} and their products up to order k^2Z^2, Eq. (15) yields

$$\Gamma_n^{(2)}\approx\tfrac{10}{9}\Gamma'(n+\tfrac{1}{2})\sqrt{E_R/U_0} . \tag{16}$$

By summing (13) and (16), one finds that the effective departure rate Γ_n^{eff} from level $|g,-\rangle\otimes|\phi_n\rangle$ is on the order of

$$\Gamma_n^{\text{eff}}\approx\Gamma'(n+\tfrac{1}{2})\sqrt{E_R/U_0} . \tag{17}$$

This rate is smaller than the optical pumping rate Γ' by a factor on the order of $\sqrt{E_R/U_0}$ for the lowest bound levels. Experimentally, it is easy to achieve values of U_0/E_R of the order of 1000. In these conditions, the effective lifetime of the lowest bound states is lengthened by a factor of the order of 30. Because the atom actually scatters photons at a rate Γ', this means that the dominant process is elastic scattering. For the figures considered above, one can estimate the number of elastic photons in the fluorescence spectrum to be on the order of 95% of the total number of scattered photons for the lowest bound states [13].

Because $\sqrt{U_0/E_R}=\hbar\Omega_v/2E_R$, one may rewrite (17) in the following form:

$$\Gamma_n^{\text{eff}}\approx\Gamma'(2n+1)\frac{E_R}{\hbar\Omega_v} . \tag{18}$$

Finally, using the same method, one can find the effective relaxation rate Γ_{nm}^{eff} for any coherence σ_{nm} between localized states n and m at the bottom of the potential well. The corresponding result is

$$\Gamma_n^{\text{eff}}\approx\Gamma'\left[\frac{n+m+1}{2}\right]\sqrt{E_R/U_0} , \tag{19}$$

or equivalently

$$\Gamma_{nm}^{\text{eff}}\approx\Gamma'(n+m+1)\frac{E_R}{\hbar\Omega_v} . \tag{20}$$

The considerable lengthening of the coherence relaxation time is due to an important transfer of coherence during an absorption-spontaneous emission cycle [14]. A semiclassical picture of the lengthening of the coherence relaxation time may also be given. This relaxation time describes how rapidly the phase of the oscillation of the atom in an optical potential well is lost. For an atom oscillating at the bottom of the potential well, the oscillating motion is interrupted by absorption-spontaneous emission cycles. However, the atom essentially returns to the potential well it has left (because the Clebsch-Gordan coefficient connecting $|g,-\rangle$ and $|e,-\frac{3}{2}\rangle$ is equal to 1) with only a small change of momentum. If this change of momentum remains small compared to the average momentum, the atomic motion is only slightly perturbed and it thus takes several absorption-spontaneous emission cycles before the oscillation is interrupted or loses the memory of its initial phase.

In conclusion, the preceding analysis shows that one should expect a considerable lengthening of T_1 and T_2 relaxation times for atoms in bound vibrational levels in the limit of deep potential wells. The lengthening of these relaxation times shows also that the boundary between the "oscillating regime" and the "jumping regime" [10] may sometimes be subtle. For example, it seems reasonable to consider that the system is in the oscillating regime in state $|n\rangle$ if $\Omega_v\gg\Gamma_n^{\text{eff}}$ (the atom oscillates during several periods before it actually leaves the state $|n\rangle$) even if $\Omega_v\ll\Gamma'$ (the experiment of [3] was in fact realized in this situation). In this case, one has an oscillating regime near the bottom of the potential well and a jumping regime above.

C. Damping rates for atomic variables involving continuum states

We show here that in the limit of shallow optical potentials where the population of the continuum states is not negligible, a lengthening of the relaxation time of populations of a different kind is expected. Our analysis is based on a semiclassical description of the atoms similar to the one of [10] where the atomic system is characterized by a Wigner representation $w_{\pm}(z,p,t)$ of the density matrix reduced to the ground-state Zeeman sublevels $|g,\pm\rangle$. The dynamical properties of the atomic system are then represented by a Fokker-Planck evolution equation for the distributions $w_{\pm}$. In particular, the eigenvalues of the associated Fokker-Planck operator give access to the damping time constants of the populations. Nonetheless, it is not sufficient to calculate the whole spectrum of the Fokker-Planck operator to have an immediate estimate of the widths of the resonances in the probe transmission spectrum. Indeed, as previously emphasized, only a few number of evolution modes are excited by the probe beam and are of interest in the probe transmission spectra. As will be shown in detail in Sec. II E 4 the probe can excite eigenfunctions of the Fokker-Planck equation which satisfy the equation

$$-\lambda w = D_0 \frac{\partial^2 w}{\partial p^2} , \tag{21}$$

where $D_0=\frac{11}{18}\hbar^2k^2\Gamma'\approx\hbar^2k^2\Gamma'/2$ is the momentum diffusion coefficient, w is the eigenfunction, and $-\lambda$ is the associated real negative eigenvalue. In order to determine the actual form of w, it is necessary to associate Eq. (21) with boundary conditions which take into account the characteristics of the probe interaction. It turns out that the probe excitation exhibits a cutoff in the momentum space for a value p_0 which is independent on the potential depth U_0, provided that the potential is sufficiently shallow (see Sec. II E 4). This property yields

$$w(p)=\cos(\sqrt{\lambda/D_0}p) , \tag{22}$$

with

$$\lambda \approx \frac{\pi^2 D_0}{p_0^2} , \tag{23}$$

where p_0 denotes the typical momentum associated with the typical highest continuum state excited by the probe beam. As shown in Sec. II E 4 (a), a typical value is $p_0\approx 100\hbar k$. It gives $\lambda\approx 10^{-3}\Gamma'$, which is much less than the Lamb-Dicke estimate (17) applied to the case of shallow optical potentials. It can be noticed from (21) that these very long damping times for the populations are associated with the very slow diffusion-induced relaxation in momentum space of a mode excited by the probe, in a regime where the cooling friction force is unefficient. Note, however, that our theoretical investigation does not take into account the Doppler cooling friction force (characterized by a friction coefficient α_D). This effect actually constrains the damping rate of the populations to be larger than α_D/M, and thus puts a lower limit on Eq. (23). It may be noticed that this influence of the continuum states on the dynamical properties of atoms in 1D optical molasses occurs in a range of parameters close to the threshold of the sub-Doppler cooling mechanism.

D. Dynamical properties of the atomic medium

As shown in [1], it is possible to write a Bloch equation for the ground-state part σ of the density matrix taking into account both the internal (Zeeman sublevels) and the external (center-of-mass position and momentum) atomic degrees of freedom. It is convenient to write this equation in the form

$$\dot{\sigma} = L\cdot\sigma , \tag{24}$$

where L is an operator acting on the density matrix. This operator describes the interaction between atoms and pump beams and encloses all the dynamical properties of the atomic medium. In particular, the eigenvalues of L represent the damping and evolution rates of populations and coherences. Note, however, that the eigenmodes generally involve a large number of density matrix elements, so that it is not possible to associate a damping rate to a given population or coherence. As will be shown in Sec. II, these eigenmodes and eigenvalues play a key role in the description of all the dynamical properties of the atoms, and are the central point of our theoretical treatment.

II. ATOMS IN THE PRESENCE OF THE PROBE BEAM

A. General

In addition to the cooling pump beams, a weak probe beam of amplitude E_p and frequency $\omega_p=\omega+\delta$ ($|\delta|\ll\omega$) propagating along the $+z$ direction is sent through the atomic medium (Fig. 2). The linear polarization of the probe $\mathbf{e}_p$ can be either parallel (along Ox) or orthogonal (along Oy) to the one of the pump beam which propagates in the same direction. In the following, we will refer to these two polarization configurations as the $\aleph=\parallel$ and $\perp$ configurations. Because we consider a pump-probe experiment, all the quantities which appear in this section will be written to first order in the small parameter:

$$\varepsilon=\frac{E_p}{E_0}\ll 1 . \tag{25}$$

We thus study the linear response of the system to the probe. In the experimental situation of Fig. 2, one may have access to several physical signals. We study two of them in the following. The first one is the variation of the probe transmission versus ω_p. The second one corresponds to four-wave mixing optical phase conjugation [15]. This process is associated with absorption of photons from the counterpropagating cooling beams, amplification of the probe and generation of a wave of frequency $2\omega-\omega_p$ propagating in the direction opposite to the direction of the probe. Such a wave can be detect-

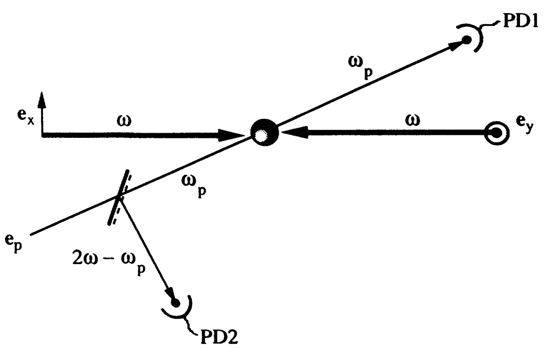

FIG. 2. Schematic experimental setup for pump-probe experiments. In addition to the cooling wave at frequency ω, a weak probe beam having linear polarization $\mathbf{e}_p$ and frequency ω_p is sent through the atomic medium (represented by a graduated sphere). By monitoring the probe intensity with photodiode PD1 as a function of the probe frequency, one has access to the probe transmission spectrum. The phase-conjugate reflected beam (frequency $2\omega-\omega_p$) can also be measured by means of photodiode PD2 (and of a plate located on the path followed by the probe beam).

ed by introducing a plate on the path followed by the probe (Fig. 2). Recently, such a signal has been observed in experiments on 1D optical molasses [16].

In the linear regime [4], the characteristics of the system (position of the resonances, damping times, etc.) are only determined by the unperturbed eigensystem of the Bloch equation (i.e., in the absence of a probe). The information that can be obtained from such a situation concerns the dynamics of the 1D optical molasses. More precisely, the direct application of the *linear-response theory* shows that the transmission of the probe beam of frequency ω_p can be calculated from the Fourier component at frequency ω_p of the function $\Theta(\tau)\langle[D_p^-(0),D_p^+(-\tau)]\rangle$. In this expression $\Theta(\tau)$ is the Heaviside function [$\Theta(\tau)=0$ if $\tau<0$ and $\Theta(\tau)=1$ if $\tau>0$], $D_p^+=(\mathbf{d}^+\cdot\mathbf{e}_p)e^{ikZ}$ ($\mathbf{d}^+=P_e\mathbf{d}P_g$ where P_e and P_g are the projectors onto the excited state and ground state, respectively), $D_p^-=(D_p^+)^\dagger$, and $D_p^+(-\tau)$ corresponds to the evolution of D_p^+ between 0 and $-\tau$ in the Heisenberg representation under the effect of the trapping beams and of the radiative relaxation. The average value of the commutator is taken in the steady state of the system in the absence of a probe. Such a result clearly shows that the positions and widths of the resonances observed on the probe transmission depend only on the zeroth-order solution and *the only effect of the probe is to excite some particular dynamical modes of the optical molasses.* The information that can be obtained from probe transmission are thus of the same kind as those obtained by monitoring the fluorescence spectrum [the line shape then depends on the Fourier transform of correlation functions of the type $\langle D_f^+(\tau)D_f^-(0)\rangle$ where f now corresponds to the polarization component and direction of analysis of the fluorescence [17]]. Similarly, the wave generated in the backward direction through phase conjugation has an intensity which depends on the square of the Fourier component of functions like $\Theta(\tau)\langle[D_{\mathrm{PC}}^-(0),D_p^-(-\tau)]\rangle$ where the index PC refers to the phase-conjugate polarization and direction [18].

All the experimental techniques considered above (probe transmission, optical phase conjugation, or fluorescence) thus give access to the dynamics of the 1D optical molasses. However, each of these experiments may be sensitive to a different combination of the eigenmodes. For example, the eigenmode associated with the steady state which has an infinite lifetime is only detected through the elastic part of the fluorescence spectrum.

B. Optical Bloch equation for internal and external degrees of freedom

We follow here a procedure similar to the one of [1] for the quantum treatment of Sisyphus cooling, but in addition a probe beam is included. The reactive part of the coupling still consists of a spatially periodic potential $U_\pm(\aleph,z,t)$ depending on the atomic ground-state sublevel $|g,\pm\rangle$, but it now depends on the probe polarization and on time. Condition (8) being fulfilled, one can adiabatically eliminate optical coherences and the excited-state part of the density matrix and obtain an evolution equation for the ground-state part σ of the density matrix, taking into account both the internal (Zeeman sublevels) and the external (center-of-mass position and momentum) degrees of freedom:

$$\dot\sigma(t)=\frac{1}{i\hbar}[H(\aleph,t),\sigma(t)]+\dot\sigma(t)_{\mathrm{relax}}\ , \tag{26}$$

with

$$H(\aleph,t)=\frac{P^2}{2M}+U_-(\aleph,Z,t)|g,-\rangle\langle g,-| \\ +U_+(\aleph,Z,t)|g,+\rangle\langle g,+| \tag{27}$$

and

$$\dot\sigma(t)_{\mathrm{relax}}=-\frac{\gamma_0}{2}[A(\aleph,t)\sigma(t)+\sigma(t)A(\aleph,t)] \\ +\gamma_0\int_{-\hbar k}^{\hbar k}dp\sum_m N_m(p)B_m^\dagger(\aleph,t)e^{-ipZ/\hbar}\sigma(t) \\ \times e^{ipZ/\hbar}B_m(\aleph,t)\ , \tag{28}$$

$$A(\aleph,t)=A_-(\aleph,Z,t)|g,-\rangle\langle g,-| \\ +A_+(\aleph,Z,t)|g,+\rangle\langle g,+|\ . \tag{29}$$

As in Sec. I the Hamiltonian H contains the atomic kinetic energy and the reactive part of the atom-field coupling. The potentials $U_\pm$ differ from the potentials $U_\pm^{(0)}$ because of the probe contribution. More precisely, one has

$$U_\pm(\aleph,Z,t)=U_\pm^{(0)}(Z)+\varepsilon\{U_\pm^{(1)}(\aleph,Z)e^{-i\delta t} \\ +[U_\pm^{(1)}(\aleph,Z)]^\dagger e^{i\delta t}\}\ , \tag{30}$$

with

$$U_\pm^{(0)}(Z)=\frac{U_0}{2}[-2\pm\cos(2kZ)]\ , \tag{31a}$$

$$U_{\pm}^{(1)}(\|,Z)=\frac{U_0}{4}(-2\pm e^{2ikZ}) , \quad (31b)$$

$$U_{\pm}^{(1)}(\perp,Z)=\frac{U_0}{4}(\pm 1-2e^{2ikZ}) . \quad (31c)$$

The relaxation term corresponding to the dissipative part of the coupling has two contributions. The first one describes the departure from a given level to the others via an absorption process. The second one accounts for the reverse process of feeding one level by the others through an absorption-spontaneous emission cycle.

In presence of the probe, operators $A_{\pm}(\aleph,Z,t)$ and $B_m(\aleph,t)$ take the form

$$A_{\pm}(\aleph,Z,t)=A_{\pm}^{(0)}(Z)+\varepsilon\{ A_{\pm}^{(1)}(\aleph,Z)e^{-i\delta t} +[A_{\pm}^{(1)}(\aleph,Z)]^{\dagger}e^{i\delta t}\} , \quad (32)$$

with

$$A_{\pm}^{(0)}(Z)=\tfrac{3}{2}[2\mp\cos(2kZ)] , \quad (33a)$$

$$A_{\pm}^{(1)}(\|,Z)=\tfrac{3}{4}(2\mp e^{2ikZ}) , \quad (33b)$$

$$A_{\pm}^{(1)}(\perp,Z)=\tfrac{3}{4}(\mp 1+2e^{2ikZ}) , \quad (33c)$$

$$B_m(\aleph,t)=B_m^{(0)}(Z)+\varepsilon\{B_m^{(1)}(\aleph,Z)e^{i\delta t}\} , \quad (34)$$

with

$$B_0^{(0)}(Z)=\cos(kZ)|g,+\rangle\langle g,-| +i\sin(kZ)|g,-\rangle\langle g,+| , \quad (35a)$$

$$B_{\pm}^{(0)}(Z)=\frac{1}{2\sqrt{2}}(e^{ikZ}\mp e^{-ikZ})\Lambda^{(\pm)} , \quad (35b)$$

$$B_0^{(1)}(\|,Z)=\tfrac{1}{2}e^{-ikZ}[|g,+\rangle\langle g,-|-|g,-\rangle\langle g,+|] , \quad (35c)$$

$$B_{\pm}^{(1)}(\|,Z)=\mp\frac{1}{2\sqrt{2}}e^{-ikZ}\Lambda^{(\pm)} , \quad (35d)$$

$$B_0^{(1)}(\perp,Z)=\tfrac{1}{2}e^{-ikZ}[|g,+\rangle\langle g,-|+|g,-\rangle\langle g,+|] , \quad (35e)$$

$$B_{\pm}^{(1)}(\perp,Z)=\frac{1}{2\sqrt{2}}e^{-ikZ}\Lambda^{(\pm)} , \quad (35f)$$

where

$$\Lambda^{(q)}=(2-q)|g,-\rangle\langle g,-|+q|g,+\rangle\langle g,+| . \quad (36)$$

The integral is taken over the momentum p along Oz of the spontaneously emitted photon, which only takes discrete values when periodic boundary conditions in a box of finite size are used. Index m represents the projection of the photon angular momentum along Oz and functions $N_m(p)$ stand for the normalized distribution pattern for the spontaneously emitted photon [19],

$$N_{\pm 1}(p)=\frac{3}{8\hbar k}\left[1+\frac{p^2}{\hbar^2k^2}\right] , \quad (37a)$$

$$N_0(p)=\frac{3}{4\hbar k}\left[1-\frac{p^2}{\hbar^2k^2}\right] . \quad (37b)$$

C. Principle of the calculation

1. General

In order to calculate the transmission spectrum of the probe, we solve the Bloch equation (28) using perturbation theory to first order in ε and to zeroth order in γ_0/Ω_v because we assume that (7) is fulfilled. The density matrix we look for is of the form

$$\sigma=\sigma^{(0)}+\varepsilon[\sigma^{(1)}e^{-i\delta t}+(\sigma^{(1)})^{\dagger}e^{i\delta t}] . \quad (38)$$

The first step of the calculation consists in solving equation

$$L\cdot\sigma^{(0)}=0 , \quad (39)$$

with

$$L\cdot\sigma=\frac{1}{i\hbar}[H^{(0)},\sigma]-\frac{\gamma_0}{2}[A^{(0)}\sigma+\sigma A^{(0)}] +\gamma_0\int_{-\hbar k}^{\hbar k}dp\sum_m N_m(p)(B_m^{(0)})^{\dagger}e^{-ipZ/\hbar}\sigma e^{ipZ/\hbar}B_m^{(0)} \quad (40)$$

and

$$A^{(0)}=A_-^{(0)}|g,-\rangle\langle g,-|+A_+^{(0)}|g,+\rangle\langle g,+| . \quad (41)$$

To simplify the resolution of the Bloch equation, we use some symmetry properties of $H^{(0)}$ and of its eigenstates $|n,q,\mu\rangle$. The Hamiltonian $H^{(0)}$ is invariant by the symmetry groups represented by the unitary transformation $\mathcal{T}$ and $\mathcal{P}$:

$$\mathcal{T}|z\rangle\otimes|\mu\rangle=\left|z+\frac{\lambda}{4}\right\rangle\otimes|-\mu\rangle , \quad (42)$$

$$\mathcal{P}|z\rangle\otimes|\mu\rangle=|-z\rangle\otimes|\mu\rangle . \quad (43)$$

It follows that the eigenstates $|n,q,-\rangle$ and $|n,q,+\rangle$ have the same energy $E_{n,q}$ and can be expressed in terms of functions $|n,q\rangle$ which have a well-defined parity:

$$|n,q,-\rangle=|g,-\rangle\otimes|n,q\rangle , \quad (44)$$

$$|n,q,+\rangle=\mathcal{T}|n,q,-\rangle . \quad (45)$$

Finally, we can note that the Bloch index q labels the way functions $|n,q\rangle$ transform by $\mathcal{T}^2$:

$$\mathcal{T}^2|n,q\rangle=e^{iq\lambda/2}|n,q\rangle . \quad (46)$$

As shown in [1], when (7) is fulfilled it is possible to prove, using secular approximation, that $\sigma^{(0)}$ is diagonal in the basis $|n,q,\mu\rangle$. In particular every density-matrix element between two states of different Bloch index are zero (due to the invariance of $\sigma^{(0)}$ by $\mathcal{T}$). It is also possible to show that the steady-state populations only depend upon the dimensionless parameter U_0/E_R. These properties of the wave functions $|n,q,\mu\rangle$ lead to a considerable simplification of the numerical calculations.

In a second step, taking into account the effect of the probe to first order in ε, one obtains an equation of the form

$$(i\delta+L)\cdot\sigma^{(1)}=S(\aleph) \ . \tag{47}$$

We solve this equation as follows: First, the Bloch operator is diagonalized:

$$L\cdot\sigma_\lambda=-(\gamma_\lambda+i\omega_\lambda)\sigma_\lambda \ , \tag{48}$$

where σ_λ is an eigenvector of eigenvalue $-\gamma_\lambda-i\omega_\lambda$ (where $\gamma_\lambda\geq 0$ and ω_λ are real). Second, the source term $S(\aleph)$ due to the interaction with the probe is expanded on the basis of the eigenvectors σ_λ:

$$S=\sum_\lambda s_\lambda\sigma_\lambda \ . \tag{49}$$

The density matrix to first order in ε is then given by

$$\sigma^{(1)}=\sum_\lambda \frac{s_\lambda}{-\gamma_\lambda+i(\delta-\omega_\lambda)}\sigma_\lambda \ . \tag{50}$$

For the numerical calculations, the integrals over the momentum along Oz of the spontaneously emitted photon are substituted for a discrete sum since periodic boundary conditions are used for both the spontaneous emission and the band structure. In the spectra presented in this article, a box of size λ has been used so that bands are described by two Bloch vectors and spontaneous emission is assumed to occur only in the $+z$ and $-z$ directions, as well as in any direction orthogonal to Oz.

2. *Case of probe transmission spectra*

In order to calculate the probe transmission spectrum, we evaluate the polarization of the medium and calculate the power transfer $P_\aleph$ from the atoms to the probe field, normalized to ε, and neglecting linear absorption:

$$P_\aleph=-\frac{1}{\varepsilon}\overline{\mathbf{E}_p^3(\aleph)\cdot\frac{d\mathbf{P}}{dt}}$$
$$=\frac{N\hbar\Omega^2\omega l}{\sqrt{2}(\Delta^2+\Gamma^2/4)}\mathrm{Im}\{(\Delta-i\Gamma/2)\mathrm{Tr}(\wp_\aleph\sigma^{(1)})\} \ , \tag{51}$$

where N is the atomic density and l is the length of the atomic medium. $\wp_\aleph$ is an operator that only depends upon $\aleph$, equal to:

$$\wp_\aleph=(\mathbf{d}^-\cdot\mathbf{e}_p^*(\aleph))(\mathbf{d}^+\cdot\mathbf{e}_0(Z))e^{-ikZ} \ . \tag{52}$$

$\mathbf{e}_p$ ($\mathbf{e}_0$) is the polarization of the probe (pump) field, $\mathbf{d}^+$ is the dimensionless exciting part of the dipole operator ($\mathbf{d}^+=P_e\mathbf{d}P_g$) and $\mathbf{d}^-=(\mathbf{d}^+)^\dagger$.

3. *Case of phase-conjugate reflection*

The phase-conjugation reflection coefficient $R_\aleph$ is calculated in the limit of a thin atomic medium, and is given by

$$R_\aleph=\left|\frac{Nd^2\omega l}{\sqrt{2}\varepsilon_0\hbar c(\Delta+i\Gamma/2)}\mathrm{Tr}[\mathcal{J}_\aleph(\sigma^{(1)})^\dagger]\right|^2 \ , \tag{53}$$

with

$$\mathcal{J}_\aleph=[d^-\cdot\mathbf{e}_{\mathrm{PC}}^*(\aleph)][d^+\cdot\mathbf{e}_0(Z)]e^{ikZ} \ , \tag{54}$$

where $\mathbf{e}_{\mathrm{PC}}$ is the polarization of the phase-conjugate beam, orthogonal to the polarization of the probe beam. Expression (53) clearly shows that the calculation of $R_\aleph$ is very similar to the one of $P_\aleph$ since the phase-conjugate reflectivity and the probe transmission are expressed in terms of the same quantities.

D. Raman transitions

We first investigate the characteristics of the Raman transitions occurring between different bands. We expect that such transitions mainly involve the lowest energy states of the optical potential, because the most important population differences occur for these levels and because most of the atoms occupy these bands in steady state. For these levels, the distance between adjacent band states is approximately constant, of the order of $\hbar\Omega_v$. We can thus estimate that Raman resonances will occur around $\delta=m\Omega_v$ (m integer number). As a consequence, in the limit where (7) is fulfilled and for $\delta\approx m\Omega_v$, a coherence $\langle n,q|\sigma|n+m,q\rangle$ ($m\neq 0$) is mainly coupled to a coherence $\langle n',q'|\sigma|n'+m',q'\rangle$ with $m=m'$ (secular approximation). It is thus possible to analyze independently for each value of $m\neq 0$ the different Raman resonances involving transitions from bands n to bands $n+m$. We then obtain the Raman spectrum with peaks centered around $\delta=m\Omega_v$.

The source term used for the calculation of Raman resonances is

$$\langle n,q,\mu|S|n+m,q,\mu\rangle$$
$$=-\frac{1}{i\hbar}\langle n,q,\mu|U_\mu^{(1)}|n+m,q,\mu\rangle(\pi_{n+m,q}^{(0)}-\pi_{n,q}^{(0)})+\frac{\gamma_0}{2}\langle n,q,\mu|A_\mu^{(1)}|n+m,q,\mu\rangle(\pi_{n+m,q}^{(0)}+\pi_{n,q}^{(0)})$$
$$-\gamma_0\sum_{n',q',\sigma'}\int_{-\hbar k}^{\hbar k}dp\sum_m N_m(p)\langle n,q,\mu|(B_m^{(1)})^\dagger e^{-ipZ/\hbar}|n',q',\mu'\rangle\langle n',q',\mu'|B_m^{(0)}e^{ipZ/\hbar}|n+m,q,\mu\rangle\pi_{n',q'}^{(0)} \ . \tag{55}$$

The first term is associated with the probe-induced coupling between levels n and $n+m$ and involves the population difference between these levels. This term corresponds to the usual contribution to Raman resonances. The second and third terms describe the effect of the probe on the radiative relaxation part of the Bloch equations. These terms, which exist even when there are no population differences between the levels, correspond to the radiative relaxation-induced extra resonances considered by Bogdan, Downer, and Bloembergen [20] for the case of four-wave mixing and which have been recently observed on probe transmission (two-wave mixing resonances) [21,22].

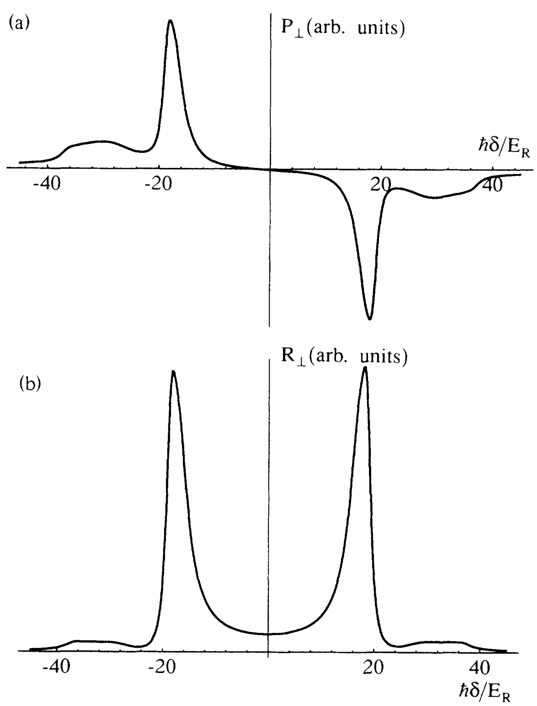

FIG. 3. Raman spectra for probe transmission and phase conjugation in the $\aleph=\perp$ polarization case. These spectra were obtained for a detuning $\Delta=-10\Gamma$, $U_0/E_R=100$, by considering the first 40 band states with Bloch index $q=0,1$. Only the first Raman resonances and the first overtones are represented. (a) Probe transmission spectrum. Whereas the typical pumping rate Γ' is equal to $15E_R/\hbar$, the width of the Raman resonances are on the order of $5E_R/\hbar$ because of the Lamb-Dicke effect. The Raman resonances are centered at $\delta=\omega_p-\omega\approx\pm\Omega_v$. The first overtones are much broader than the Raman resonances because of the contribution of high bound vibrational levels which are less affected by the Lamb-Dicke effect. The energy separation between these levels is less than $\hbar\Omega_v$, so that the overtones are not exactly located at $\delta=\omega_p-\omega\approx\pm2\Omega_v$, due to the optical potential anharmonicity. (b) Phase-conjugate spectrum. This spectrum provides the same information as the probe transmission spectrum. In particular, the Raman resonances and the first overtone are clearly visible. Note that this calculation does not take into account the effects related to the saturation of the optical transition. Such effects would have a contribution independent on the probe frequency. The interference with the contribution due to the ground state only, which does not have the same sign for $\delta>0$ and $\delta<0$, can lead in experimental spectra to Raman resonances of different weights.

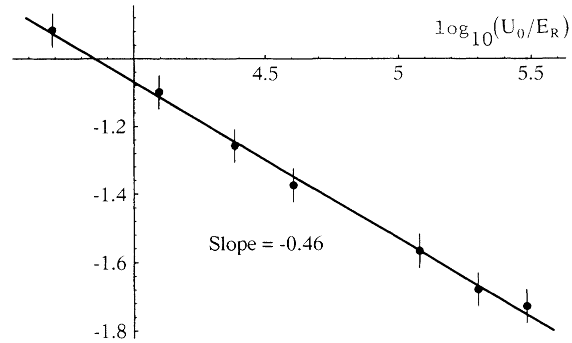

FIG. 4. Ratio of the width of the first Raman resonances to Γ' vs the dimensionless parameter U_0/E_R for a detuning $\Delta=-10\Gamma$ in the $\aleph=\perp$ polarization case (log-log representation). The variation is in agreement with the $\sqrt{E_R/U_0}$ law obtained in the Lamb-Dicke limit.

An example of theoretical Raman spectrum is shown in Fig. 3 for both probe transmission [Fig. 3(a)] and phase conjugation [Fig. 3(b)]. The resonances have been calculated for $m=1$ and 2 (first overtone). As previously mentioned, Raman spectra exhibit resonances whose width is smaller than the typical pumping rate Γ'. The dependence of the ratio of the width of the first resonance to Γ' versus the dimensionless parameter U_0/E_R is in good agreement with the simple law (19) obtained in the Lamb-Dicke limit (Fig. 4). In the range considered in Fig. 5, the position of the first Raman resonances is also in good agreement with the $\sqrt{U_0/E_R}$ law, but its exact position exhibits a slight shift compared to the value calculated for a harmonic oscillator, which is due in particular to the potential anharmonicity. In contrast, the position of the resonances is in reasonable agreement with the energy difference between two deep adjacent bands calcu-

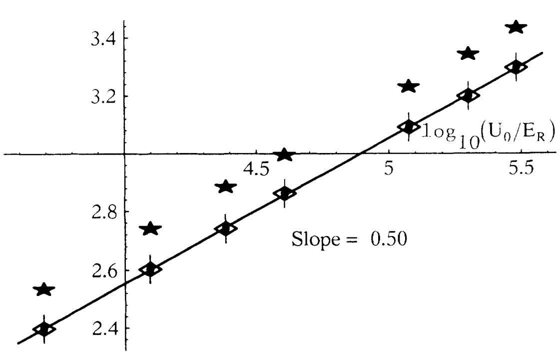

FIG. 5. Position of the first Raman resonances (represented by diamonds) vs the dimensionless parameter U_0/E_R for a detuning $\Delta=-10\Gamma$ in the $\aleph=\perp$ polarization case (log-log representation). The position dependence is in very good agreement with the $\sqrt{U_0/E_R}$ law corresponding to a harmonic approximation. However, the exact position is slightly different from the expected Ω_v value (represented by stars). This shift is due in particular to anharmonicity of the optical potential.

lated from the exact potential. However, for small values of U_0/E_R ($U_0/E_R < 50$), the Raman resonances result from a sum of curves centered at different locations because of the potential anharmonicity so that the comparison becomes meaningless. In addition, for large values of U_0/E_R ($U_0/E_R > 500$) the shape of the resonances clearly demonstrates the occurrence of different relaxation time constants associated with the different damping rates of the eigenmodes of the Bloch operator.

The amplitude I_2 of the first overtone is always much smaller than the amplitude of the first Raman resonance I_1, and the ratio I_2/I_1 decreases when U_0/E_R increases. This variation is a consequence of the Lamb-Dicke effect. More precisely, if terms of the order of $k\Delta Z \approx (E_R/U_0)^{1/4}$ such as $\langle \phi_{n+1}|kZ|\phi_n\rangle$ (obtained in the expansion of terms like e^{2ikZ} found in $U_\pm^{(1)}$ and $A_\pm^{(1)}$ in power of kZ) are sufficient to induce the first Raman resonance, one should consider terms of the order of $(k\Delta Z)^2$ such as $\langle \phi_{n+2}|(kZ)^2|\phi_n\rangle$ to excite the first overtone. In the Lamb-Dicke regime where $k\Delta Z \ll 1$, the ratio I_2/I_1 is thus expected to decrease when U_0/E_R increases. Moreover, in the case of very deep potential wells (large values of U_0) the contribution of the lowest bands to the first overtone can become negligible compared to the contribution of higher bound vibrational levels which are less populated. These levels, which cannot be approximated by harmonic potential eigenstates, are separated by less than Ω_v so that the center of the first overtone is not located around $2\Omega_v$ but appears closer to the first Raman resonance. These predictions are in good agreement with a very recent experiment [16] where overtones have been observed.

The fact that optical phase conjugation displays a resonant enhancement when δ coincides with the energy difference between two bound states in the optical potential is very similar to the resonant enhancement of nonlinear susceptibility in quantum wells [23]. One might in fact describe the present system as an *atomic quantum well.*

One further possibility with the Raman resonances would be the observation of substructures in the Raman spectra due to the anharmonicity of the potential. It turns out that such structures arise only for large detunings and small values of U_0/E_R ($U_0/E_R = 40$ and $\Delta = -20\Gamma$ are typical) for which the substructures are not hidden by the width of the different contributions. In contrast, it seems extremely difficult to obtain evidence for the occurrence of a *band* structure different from the structure of energy levels in a single potential well. Indeed, the width of the lowest bands due to tunneling transition to an adjacent potential well (through the potential barrier) is much smaller than the width induced by interaction with light.

E. Rayleigh resonances

As experimentally shown in [3], probe transmission spectra display amazing resonances at the center of the spectrum where $\delta \approx 0$. These resonances have uncommon shapes, very steep slopes, and depend dramatically on the probe polarization. In fact, these resonances are strongly connected to the two-wave mixing resonances (also called stimulated Rayleigh or two-beam coupling resonances) that have been observed in atomic vapors [24,25,21]. These resonances are generally associated with the excitation of a slow atomic observable by the combined effect of a pump beam and a probe beam. The subsequent interaction of the pump beam with the atomic observable which is not in phase with the excitation (because of the atomic response time) leads to an energy transfer between probe and pump which exhibits a resonance when the two frequencies differ by the inverse of the atomic response time. Similar effects occur in the molasses with the additional interest of the existence of effects due to atom localization and the additional complexity of the existence of several response times associated with the various eigenstates of the Bloch operator. It is the aim of this section to give a detailed interpretation of such resonances for the case of a $J_g = \frac{1}{2} \to J_e = \frac{3}{2}$ atomic transition.

1. Adiabatic states

In order to give simple physical pictures and to simplify numerical calculations, we will not base our description here on the eigenstates of the Hamiltonian $H^{(0)}$ in the absence of probe but on the eigenstates of the total Hamiltonian H. In the limit where (7) is fulfilled, it is possible to use an adiabatic approximation [26], so that the eigenstates $\overline{|n,q,\mu\rangle}$ of H can easily be expressed in terms of those of $H^{(0)}|n,q,\mu\rangle$:

$$\overline{|n,q,\mu\rangle} = |n,q,\mu\rangle + \varepsilon[\,|n,q,\mu\rangle_+^{(1)} e^{-i\delta t} + |n,q,\mu\rangle_-^{(1)} e^{i\delta t}\,] \,, \tag{56}$$

with

$$|n,q,\mu\rangle_+^{(1)} = \sum_{n'\neq n} \frac{\langle n',q,\mu|U_\mu^{(1)}|n,q,\mu\rangle}{E_{n,q}-E_{n',q}} |n',q,\mu\rangle \,, \tag{57a}$$

$$|n,q,\mu\rangle_-^{(1)} = \sum_{n'\neq n} \frac{\langle n',q,\mu|(U_\mu^{(1)})^\dagger|n,q,\mu\rangle}{E_{n,q}-E_{n',q}} |n',q,\mu\rangle \,. \tag{57b}$$

In this basis, it is then possible to use the secular approximation, so that the density matrix modified by the probe is diagonal. It follows that only the populations of the adiabatic band states $\overline{|n,q,\mu\rangle}$ are modified, and simple physical pictures can be obtained.

The source term can be split into two different parts:

$$S = S_{\text{diss}} + S_{\text{reac}} \,, \tag{58}$$

with

$$\overline{\langle n,q,\mu|}S_{\mathrm{diss}}\overline{|n,q,\mu\rangle}=\gamma_0\langle n,q,\mu|\,A_{\mu}^{(1)}|n,q,\mu\rangle\overline{\pi}_{n,q}^{(0)}$$
$$-\gamma_0\sum_{n',q',\mu'}\int_{-\hbar k}^{\hbar k}dp\sum_{m}N_m(p)\langle n,q,\mu|(B_m^{(1)})^{\dagger}e^{-ipZ/\hbar}|n',q',\mu'\rangle\langle n',q',\mu'|B_m^{(0)}e^{ipZ/\hbar}|n,q,\mu\rangle\overline{\pi}_{n',q'}^{(0)} \tag{59}$$

and

$$\overline{\langle n,q,\mu|}S_{\mathrm{reac}}\overline{|n,q,\mu\rangle}=\gamma_0[\langle n,q,\mu|\,A^{(0)}|n,q,\mu\rangle_{+}^{(1)}+{}_{-}^{(1)}\langle n,q,\mu|\,A^{(0)}|n,q,\mu\rangle]\overline{\pi}_{n,q}^{(0)}$$
$$-\gamma_0\sum_{n',q',\mu'}\int_{-\hbar k}^{\hbar k}dp\sum_{m}N_m(p)\beta(n,q,\mu;n',q',\mu';p)\overline{\pi}_{n',q'}^{(0)}\ , \tag{60}$$

where

$$\beta(n,q,\mu;n',q',\mu';p)={}_{-}^{(1)}\langle n,q,\mu|(B_m^{(0)})^{\dagger}e^{-ipZ/\hbar}|n',q',\mu'\rangle\langle n',q',\mu'|B_m^{(0)}e^{ipZ/\hbar}|n,q,\mu\rangle$$
$$+\langle n,q,\mu|(B_m^{(0)})^{\dagger}e^{-ipZ/\hbar}|n',q',\mu'\rangle\,{}_{+}^{(1)}\,\langle n',q',\mu'|B_m^{(0)}e^{ipZ/\hbar}|n,q,\mu\rangle$$
$$+\langle n,q,\mu|(B_m^{(0)})^{\dagger}e^{-ipZ/\hbar}|n',q',\mu'\rangle\,{}_{-}^{(1)}\,\langle n',q',\mu'|B_m^{(0)}e^{ipZ/\hbar}|n,q,\mu\rangle$$
$$+\langle n,q,\mu|(B_m^{(0)})^{\dagger}e^{-ipZ/\hbar}|n',q',\mu'\rangle\langle n',q',\mu'|B_m^{(0)}e^{ipZ/\hbar}|n,q,\mu\rangle_{+}^{(1)}\ . \tag{61}$$

Despite the apparent complexity of this expression, the physical interpretation is rather clear and allows us to understand the features of the central resonances. The dissipative part of the source term accounts for the modification of the *optical pumping in the presence of the probe* on the populations of the *eigenstates in the absence of the probe.* The reactive part of the source term stands for the effect of the *optical pumping in the absence of the probe* on the population of the *eigenstates modified by the probe.* These effects will be discussed in detail in the following for the two polarization configurations of the probe.

2. *Evolution of populations: Global analysis*

The precise influence of the probe beam on the populations of the vibrational levels is complex and will be discussed in the following. In a first step, we want to give simple ideas about the way these population modifications lead to probe amplification or absorption. For this purpose, it is enough to characterize these population modifications by use of simple symmetry considerations. Due to the invariance of the L operator by $\mathcal{T}$ (translation by $\lambda/4$ along Oz and exchange of internal state)

$$\mathcal{T}L\mathcal{T}^{+}=L\ , \tag{62}$$

the properties of the source terms for the two polarization configurations of the probe

$$\mathcal{T}S(\parallel)\mathcal{T}^{+}=S(\parallel)\ , \tag{63a}$$

$$\mathcal{T}S(\perp)\mathcal{T}^{+}=-S(\perp) \tag{63b}$$

provide important information about the density-matrix modification $\sigma^{(1)}$. Indeed, combining (47), (62), and (63), we obtain

$$\mathcal{T}\sigma_{\parallel}^{(1)}\mathcal{T}^{+}=\sigma_{\parallel}^{(1)}\ , \tag{64a}$$

$$\mathcal{T}\sigma_{\perp}^{(1)}\mathcal{T}^{+}=-\sigma_{\perp}^{(1)}\ , \tag{64b}$$

which clearly shows that in the $\aleph=\parallel$ configuration the population modifications are *identical* in each potential well and the total population of a given well is *unchanged* [Fig. 6(b)], whereas in the $\aleph=\perp$ configuration the population modifications of the two potentials are *opposite* and there occurs a *net population transfer* from one potential to the other [Fig. 6(c)].

When calculating the power transfer $P_{\aleph}$ from the atoms to the probe field one has to calculate the mean value of the operator $\wp_{\aleph}$ [Eq. (52)] by means of the modified density matrix $\sigma^{(1)}$. For the two polarization configurations of the probe, $\wp_{\aleph}$ is given by

$$\wp_{\parallel}=\frac{\sqrt{2}}{3}(I-J_z e^{-2ikz})\ , \tag{65a}$$

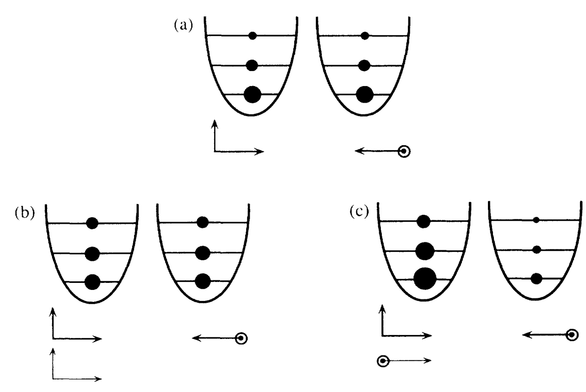

FIG. 6. Probe-induced population modifications. (a) In the absence of probe, the different optical potential wells are equally populated. (b) In the $\aleph=\parallel$ polarization configuration, the probe beam induces modifications of the population of the vibrational levels, but these modifications are the same in each potential well, so that the global population of each potential well remains constant. (c) In the $\aleph=\perp$ polarization configuration the probe induces population transfer from one potential well to the adjacent ones, so that the global population of each potential well oscillates in time with frequency $\omega_p-\omega$.

and

$$\wp_{\perp}=\frac{\sqrt{2}}{3}(-J_z+Ie^{-2ikz})\ , \tag{65b}$$

where I is the identity operator for the internal degrees of freedom which accounts for atomic density effects and J_z is the component of the angular momentum along Oz. The terms dependent on z stand for effects due to the *backscattering* of the pump wave which counterpropagates with the probe on a *magnetization* ($\aleph=\|$) or a *density* ($\aleph=\perp$) grating. The terms independent on z represent contributions due to the copropagating pump beam interacting with a population ($\aleph=\|$) or a magnetization ($\aleph=\perp$) global modification. We now precise the interpretation and the different contributions of these terms.

a. Configuration $\aleph=\|$. Because of the conservation of the total atomic population, the first term of (65a) does not contribute to the power transfer. It follows that the central structure of the probe transmission spectrum only results from the backscattering of the counterpropagating pump wave on the magnetization grating induced by the probe. Let us describe how the magnetization grating can give rise to such a transfer.

In the absence of the probe beam, due to localization of atoms at the bottom of the potential wells associated with a given internal state $|g,+\rangle$ or $|g,-\rangle$, the atomic molasses looks like an antiferromagnetic medium, whose magnetization is alternatively positive and negative each $\lambda/4$. The presence of the probe induces population changes which are exactly the same in every potential well [Fig. 6(b)]. The resulting spatial modulation of the magnetization is thus also alternatively positive and negative each $\lambda/4$, and its amplitude varies in time with period $2\pi/\delta$. The scattering of the counterpropagating pump beam on this time-modulated magnetization results in a wave whose polarization, frequency, and direction of propagation coincide with those of the probe beam, so that it can interfere with it. The phase of the scattered wave varies with the sign of the magnetization and thus changes sign every $\lambda/4$. The reason for this phase variation is that the elementary process is a Faraday rotation of the counterpropagating pump-beam polarization around the atomic magnetization [21]. Because the sign of the rotation changes for opposite values of the magnetization, the wave scattered by the atoms having a positive magnetization experiences an intrinsic π phase shift with respect to the wave scattered by atoms having the opposite magnetization. This π phase shift compensates for the π phase shift due to the propagation of the backscattered wave between two magnetization planes which are $\lambda/4$ apart, so that the backscattered pump beam can interfere constructively with the probe beam. As shown in [21], one can obtain absorption or amplification of the probe depending on the sign of δ. The range of values of δ over which amplification or absorption is observed gives an estimate of the response times of the molasses.

To have an efficient constructive interference for the backscattered light, it is fundamental that the atoms are well localized every $\lambda/4$. If we consider, for example, the delocalized wave function of a highly excited band, the backscattering may occur from any position in the molasses, leading to a broad distribution for the phase shift due to propagation. The resulting effect will be a destructive interference on the backscattered wave. The existence of the central resonance for this polarization configuration has thus two important consequences. On one hand it proves the existence of well-localized states near the bottom of the potential wells. On the other hand it shows that there is a large-scale spatial order with atoms having opposite magnetizations every $\lambda/4$. Such a structure obviously presents some analogy with an antiferromagnetic medium.

b. Configuration $\aleph=\perp$. Let us distinguish between the different contributions of the two pump waves. The copropagating pump wave is sensitive to the global magnetization of the atomic sample [Eq. (65b)]. In the absence of probe, due to the antiferromagnetic character of the molasses, the average magnetization of the sample is equal to zero. In contrast, the interaction with the probe induces net population transfers from one potential well to adjacent ones [Fig. 6(c)] which result in a net magnetization of the medium. Because the medium is now optically active [21], the copropagating pump wave undergoes a net polarization rotation (associated with a change of frequency [21]), and can interfere constructively with

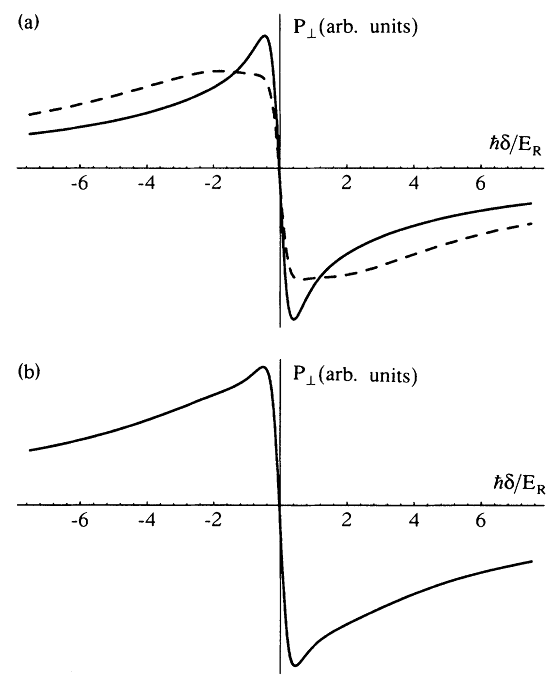

FIG. 7. Central structure of the probe transmission spectrum in the conditions of Fig. 3. (a) The contribution of the magnetization and of the density modulation are represented, respectively, by a dashed and a solid line. This figure clearly shows that both effects are important and contribute to the signal. (b) The sum of these two contributions gives a curve with a steep slope at the center and broad wings in agreement with experimental observations. The unusual shape of the central resonance is due to the existence of various time constants in the population dynamical evolution.

the probe beam. Note that this contribution does not involve atom localization, so that even excited band states contribute to the signal. The counterpropagating pump wave which has the same polarization as the probe can undergo a Bragg diffraction on the density grating induced by population transfers from one potential to the other. Note that the density grating induced by the probe has a spatial period equal to $\lambda/2$. Such a periodicity is important for having a constructive Bragg scattering in the backward direction since the phase shift due to propagation between two planes distant from $\lambda/2$ is just equal to 2π. This diffraction is also associated with a change of frequency, so that the backscattered wave can interfere constructively with the probe beam. This contribution due to the backscattering process involves atom localization. It is responsible for a significant part of the signal as can be seen in Fig. 7(a) where the relative weight of these two contributions is presented for $U_0=100E_R$. It clearly shows that both effects are important and contribute to the central structure.

3. *Dissipative effects*

The interpretation of the dissipative part of the source term will be based on semiclassical arguments, describing the effect of light on atoms at rest at a given point z. This information can then be used to obtain interesting pictures in the band model by averaging the semiclassical quantities over the spatial distribution of the band wave functions. Let us consider an atom at rest at a given point z, irradiated by the pump beams and the probe. In the case of a $J_g=\frac{1}{2}\rightarrow J_e=\frac{3}{2}$ transition, the stationary values $\pi_+(z)$ and $\pi_-(z)$ of the populations of the Zeeman sublevels $|g,+\rangle$ and $|g,-\rangle$ are solutions of the system

$$\begin{aligned} &I_+(z)\pi_-(z)=I_-(z)\pi_+(z)\ , \\ &\pi_-(z)+\pi_+(z)=1\ , \end{aligned} \tag{66}$$

where $I_+(z)$ and $I_-(z)$ are the intensities of the σ^+ and σ^- polarization component of the field at point z, normalized to the intensity of the pump field $(2E_0^2)$. Using perturbation theory to first order in ε, this system transforms into

$$\begin{aligned} &\pi_\pm(z)=\pi_\pm^{(0)}(z)+\varepsilon\pi_\pm^{(1)}(z)\ , \\ &I_\pm(z)=I_\pm^{(0)}(z)+\varepsilon I_\pm^{(1)}(z)\ , \\ &\pi_+^{(0)}(z)=\sin^2(kz)\ , \\ &\pi_-^{(0)}(z)=\cos^2(kz)\ , \\ &\pi_+^{(1)}(z)=-\pi_-^{(1)}(z)=I_+^{(1)}(z)\cos^2(kz)-I_-^{(1)}(z)\sin^2(kz)\ , \end{aligned} \tag{67}$$

which clearly shows that the modification of the steady state due to the dissipative part of the source term depends only upon the intensity components $I_\pm^{(1)}$, which are evaluated in the following.

a. Configuration $\aleph=\|$. The combination of the probe with the two pump beams leads to

$$\begin{aligned} &I_\pm^{(1)}(z)=\mp\cos(2kz-\delta t)+\cos(\delta t)\ , \\ &\pi_\pm^{(1)}(z)=\mp\sin(\delta t)\sin(2kz)\ . \end{aligned} \tag{68}$$

The resulting intensity is space and time dependent and, when averaged over the spatial extension of a band wave function, has an alternative σ^+ and σ^- dominant component. It has no net effect on the populations of the vibrational levels [Fig. 8(a)]. This result can be understood by considering the intensities $I_\pm^{(1)}(z)$ in the rotating frame

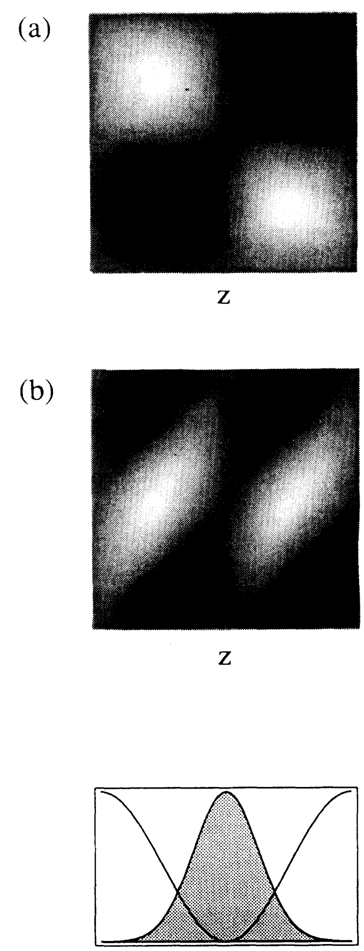

FIG. 8. Semiclassical representation of the probe-induced dissipative effects. The density plots represent the temporal evolution of $\pi_+^{(1)}(z)$. Black (white) color denotes a negative (positive) value of $\pi_+^{(1)}(z)$. It is possible to understand the effect of the probe by averaging $\pi_+^{(1)}(z)$ over the spatial extension of a band wave function (represented in gray at the bottom of the figure, for a single potential well). (a) $\aleph=\|$ polarization configuration. The average value of $\pi_+^{(1)}(z)$ for any band state is clearly equal to zero, so that the probe-induced dissipative effect does not lead to population changes. (b) $\aleph=\perp$ polarization configuration. The average value of $\pi_+^{(1)}(z)$ for any band state is nonzero and oscillates in time. The probe-induced dissipative effect thus leads to alternative population transfers from one potential well to the other. It is interesting to note that the value of $\pi_+^{(1)}(z)$ for $z=0$ is constant equal to zero, which means that an infinitely localized atom would not be affected (in the semiclassical limit) by the dissipative effects due to the probe. We have checked that the population of the lowest vibrational levels are less affected than the others for sufficiently deep potential wells.

for the probe

$$[I_{\pm}^{(1)}]_{\mathrm{RF}}(z)=1\mp\cos(2kz) , \quad (69)$$

which is nothing but the intensities due to the pump beams alone. S_{diss} is thus nothing but $-L\cdot\sigma^{(0)}$, which is by definition equal to zero, so that the dissipative effects of the probe have no influence on the probe transmission spectrum. This result is typical of a $J_g=\frac{1}{2}\rightarrow J_e=\frac{3}{2}$ atomic transition.

b. Configuration $\aleph=\perp$. Combining the probe with the two pump beams, we obtain

$$\begin{aligned} I_{\pm}^{(1)}(z)&=\cos(2kz-\delta t)\mp\cos(\delta t) , \\ \pi_{\pm}^{(1)}(z)&=\pm\tfrac{1}{2}[\cos(4kz-\delta t)-\cos(\delta t)] . \end{aligned} \quad (70)$$

The resulting intensity is space and time dependent and, when averaged over the spatial extension of a band wave function, has an alternative σ^+ and σ^- dominant component. Its net effect on the populations corresponds to an alternative departure from the wells of potential $U_{+}^{(0)}$ to the wells of potential $U_{-}^{(0)}$ [Fig. 8(b)]. It is interesting to note that (70) is equal to zero for $z=m\lambda/4$ (m is an integer), which corresponds to the bottom and the top of the potential wells. It follows that the population of an infinitely localized atom would not be modified by the dissipative effects of the probe. The departure from one potential to the other is due to the optical pumping induced by the probe beam. Typical evolution times on the order of γ_0^{-1} are found for this process which involves the global equilibrium between levels $|g,-\rangle$ and $|g,+\rangle$.

4. Reactive effects

The reactive part of the source term accounts for the time-dependent modification of the potentials $U_{\pm}$ and of the band wave functions due to the interaction with the probe. Because of the probe-induced translation of the optical potential and modification of its curvature, the steady-state atomic populations are no longer in equilibrium with the pump beam. Optical pumping due to the cooling beam then tends to adapt the populations to the time-dependent shape of the potentials. We discuss, in the following, the two polarization configurations of the probe, the way potentials are modified, their effect on the populations, and the different time constants involved in the atomic response to the probe perturbation.

a. Configuration $\aleph=\|$. The periodic perturbation (period $T=2\pi/\delta$) of the potentials induced by the probe is represented in Fig. 9(a) at four different times. At $t=0$ (0.5 T) the depth of potentials U_- and U_+ are modified by the same quantity and are smaller (larger) than U_0. As a result, the atomic populations in each potential will be modified to reach the equilibrium state corresponding to the new depth of the potentials. Due to the symmetry between potentials U_- and U_+, this equilibrium does not imply a global population transfer from one potential to the other. At $t=0.25$ T (0.75 T) the depth of potentials U_- and U_+ is not modified, but their bottom is translated by a small amount on the left (right). This translation is also responsible for a modification of the steady-state populations. The typical time constant involved in these processes is the time necessary to reach the equilibrium between the populations of the lowest band states which are affected by the probe-induced modifications of the potential. In order to estimate this time constant (related to the width of the central resonance), we distinguish two limiting cases.

(i) Case of deep potential wells. In the case of deep potential wells, the total steady-state population of the continuum states is negligible [1] and the coupling between the bound and the continuum states is very weak. As a consequence, the dynamical properties of the system are mainly due to the response time of the lowest bands population, which is considerably reduced due to the Lamb-

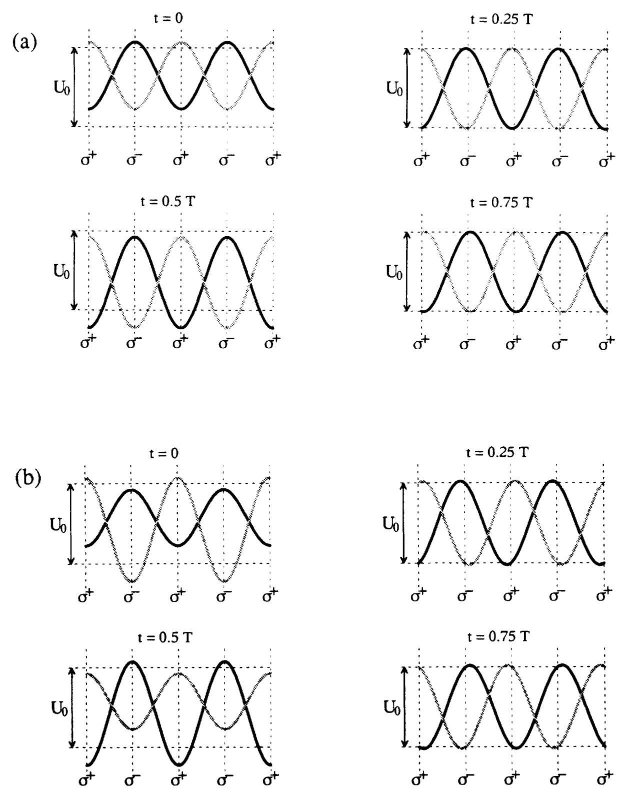

FIG. 9. Probe-induced modifications of the optical potential. The dashed lines permit us to localize the potential wells in absence of probe. The black (gray) potential corresponds to the $|g,+\rangle$ ($|g,-\rangle$) ground-state Zeeman sublevel. The local polarization of the cooling wave is indicated. We have represented the potential shapes at four different times during a period $T=2\pi/|\omega-\omega_p|$. At $t=0$ and 0.5 T the potential depth is modified, whereas at $t=0.25$ and 0.75 T the potential wells are translated in space. These potential changes lead to population modifications due to the tendency of the cooling beams to adapt the population distribution to the new potential shape. (a) $\aleph=\|$ polarization configuration. The potential wells associated with the two Zeeman sublevels are simultaneously modified so that the population changes are the same in each potential well. (b) $\aleph=\perp$ polarization configuration. The potential wells associated with the two Zeeman sublevels are modified with a phase delay of π, so that the population changes are opposite in adjacent potential wells.

Dicke effect (see Sec. I B). The width of the central structure is thus expected to be on the order of Γ_0^{eff} [Eq. (17)] [Fig. 10(a)].

(ii) Case of shallow optical potential wells. As mentioned in Sec. I C, the physical characteristics of the atomic medium in the case of shallow optical potential is significantly different from the case of deep potentials. In the present situation, the total steady-state population of the continuum and its coupling with the bound states are not negligible. In order to estimate the typical damping time of the populations, we consider a semiclassical description of the system in terms of Wigner distributions $w_\pm$ independent on z (see Sec. I C) which satisfy a Fokker-Planck equation [10]. Similarly to the description of the atomic system in terms of a Bloch operator (Sec. I D) the damping rates for atomic variables are here given by the eigenvalues of the associated Fokker-Planck operator. Due to symmetry properties of the system by exchange of the two internal Zeeman sublevels (unitary transformation $\mathcal{T}$ of Sec. I B), the eigenfunctions of the Fokker-Planck operator which are excited by the probe in the $\aleph = \parallel$ polarization configuration satisfy (63.a):

$$w_+(p) = w_-(p) = w(p) \tag{71}$$

Following [10], the corresponding eigenvalue problem can be written:

$$-\lambda w \approx D_0 \frac{\partial^2 w}{\partial p^2} \tag{72}$$

where $D_0 = \frac{11}{18}\hbar^2 k^2 \Gamma' \approx \hbar^2 k^2 \Gamma'/2$ is the momentum diffusion coefficient and $-\lambda$ is the real negative eigenvalue associated with w. As mentioned in Sec. I C, w is given by equation (22). The corresponding value for λ is given in equation (23) where p_0 stands for the maximum momentum excited by the probe beam. In order to evaluate this quantity, we note that the reactive part of the source term (60) which depends on the modification of the band states decreases in momentum space as $1/p$ [the denominator of (57) is proportional to $1/p$ for a continuum state corresponding to momentum p]. A rigorous calculation based on the Bloch equations shows that a cutoff in momentum space arises for $p_0 \approx 60$ and that it is relatively insensitive to the potential depth for small values of U_0/E_R. This is not surprising since both the continuum states and the distribution of population in the continuum are only slightly affected by the optical potential. The calculation also proves that the exact eigenvalues are in good agreement with (72) and that the eigenstates $w(p)$ are consistent with a sinusoidal shape, even if their amplitude decreases with p to satisfy $\int w(p)dp = 0$ (conservation of the total population). As expected, these modes are coupled with the lowest bound states. This condition is necessary for the eigenmodes to contribute to the probe transmission spectrum because the central resonance arises from a backscattering of a pump wave onto a magnetization grating modulation (Sec. II E 2 a), so that only the well-localized states play a role in the process. The occurrence of such long damping times on the central resonance is visible on Fig. 10(b) where we also note an inversion of this central structure.

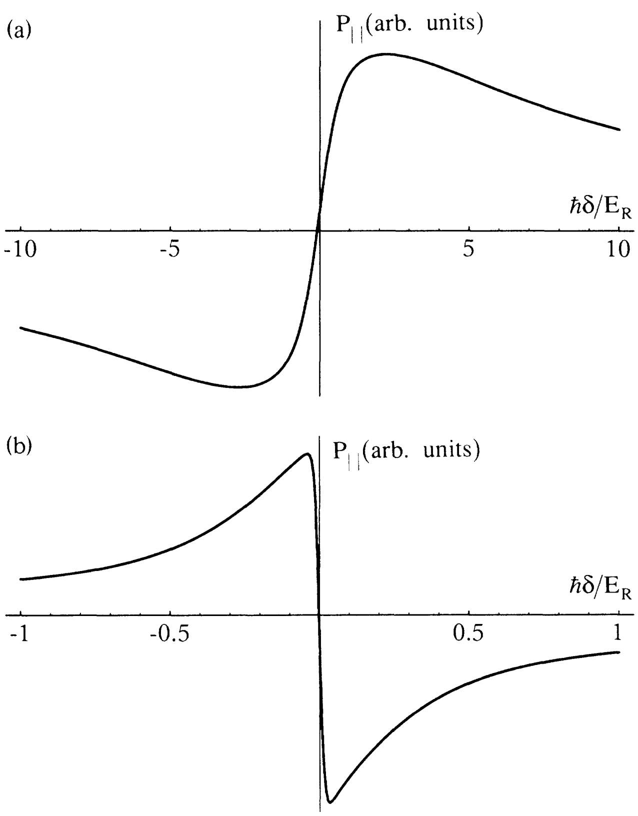

FIG. 10. $\aleph = \parallel$ polarization configuration. Dependence of the shape of the central resonance on the potential depth. When not mentioned, the conditions are the same as in Fig. 3. (a) Case of deep potential wells ($U_0/E_R = 200$, $\hbar\Gamma' = 30E_R$). The central resonance looks like a dispersion of width $\approx \Gamma_0^{\text{eff}} \approx 1E_R/\hbar$. (b) Case of shallow optical potential wells ($U_0/E_R = 40$, $\hbar\Gamma' = 6E_R$). The central resonance looks like a dispersion of width $\approx 10^{-3}\ \Gamma' \approx 0.03E_R/\hbar$. Note the change of sign of the resonance in the two situations.

b. Configuration $\aleph = \perp$. The periodic perturbation (period $T = 2\pi/\delta$) of the potentials induced by the probe is represented on Fig. 9(b) at four different times. At $t = 0$ and 0.5 T, the depth of potentials U_- and U_+ are differently modified: one is larger than U_0, the other is smaller. As a result the atomic populations will adjust to reach the equilibrium state corresponding to the new depth of the potentials, but contrary to the previous case, this equilibrium requires a net population transfer from one potential to the other. At $t = 0.25$ and 0.75 T, the depth of potentials U_- and U_+ are not modified, but their bottom are translated (in different directions), which also lead to population modifications. Similarly to the previous polarization configuration, we estimate the width of the central resonance in two limiting cases.

(i) Case of deep potential wells. In contrast with the $\aleph = \parallel$ polarization configuration, the atomic system here goes towards equilibrium by two means. First, dynamical population modifications occur to adapt the population distribution to the modulated depth of the potential. Second, this adaptation implies a net population transfer from one potential to the other. In the case of deep potential wells where the dynamical properties of the system are mainly due to the response time of the lowest bands populations, one expects these processes to occur, respectively, at a rate $\Gamma_0^{(1)}$ and $\Gamma_0^{(2)}$ (see Sec. I B), which are both on the order of Γ_0^{eff} and smaller than Γ' because of the Lamb-Dicke effect.

The actual shape of the central structure results from the combined effect of the dissipative and the reactive part of the source term. It is thus the superposition of two structures having a width on the order of Γ_0^{eff} and of γ_0 (see Sec. III D 3 *b*), which leads to an unusual cliff shape [Fig. 11(a)].

(ii) Case of shallow optical potential wells. Similarly to the $\aleph=\parallel$ polarization case, the eigenfunctions of the Fokker-Planck operator which are excited by the probe in the $\aleph=\perp$ configuration satisfy (63b)

$$w_+(p)=-w_-(p)=w(p) . \tag{73}$$

Following [10], the corresponding eigenvalue problem can be written

$$(\gamma_0-\lambda)w \approx D_0 \frac{\partial^2 w}{\partial p^2} \tag{74}$$

and the same reasoning as in the previous polarization case yields

$$\lambda \approx \gamma_0 . \tag{75}$$

This result, which is in good agreement with the exact calculation indicates that in the case of shallow optical potentials and of the $\aleph=\perp$ polarization configuration, the central structure is no longer cliff-shaped but rather looks like a dispersion of width $\approx\gamma_0$ for which the Lamb-Dicke effect plays no significant role [Fig. 11(b)]. It is also interesting to note that the contribution to the central resonance of the backscattering on the time-modulated density grating becomes very small compared to the contribution due to the forward scattering on the magnetization grating.

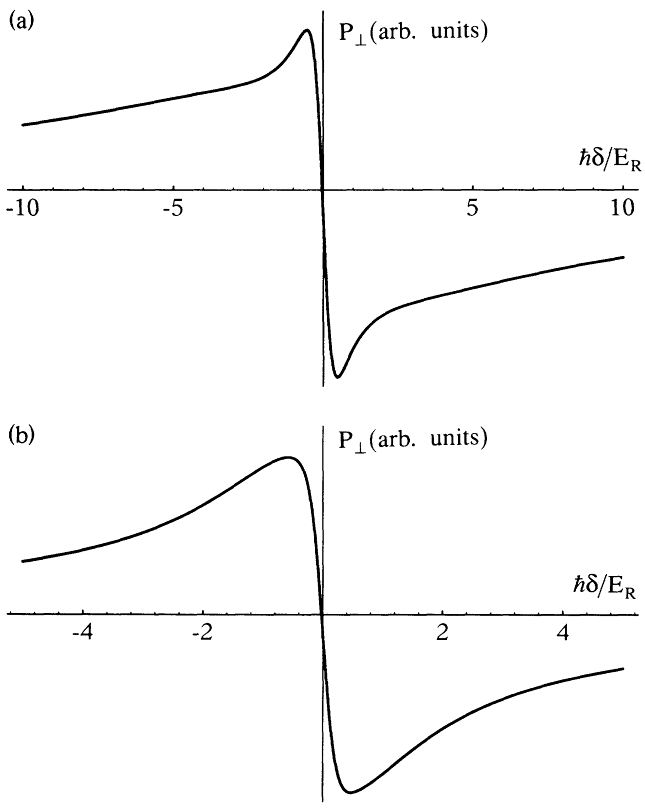

FIG. 11. $\aleph=\perp$ polarization configuration. Dependence of the shape of the central resonance on the potential depth. When not mentioned, the conditions are the same as in Fig. 3. (a) Case of deep potential wells ($U_0/E_R=200$, $\hbar\Gamma'=30E_R$). The cliff-shaped central resonance results from the superposition of two structures of width $\approx\gamma_0\approx 7E_R/\hbar$ and $\approx\Gamma_0^{\text{eff}}\approx 1E_R/\hbar$. (b) Case of shallow optical potential wells ($U_0/E_R=40$, $\hbar\Gamma'=6E_R$). The central resonance looks like a dispersion of width $\approx\gamma_0\approx 1E_R/\hbar$.

III. CONCLUSION

In this paper, we have presented theoretical line shapes for probe transmission and phase-conjugate reflection in 1D lin⊥lin optical molasses. The results are in good agreement with experimental observations [3,16] and in particular prove the following points:

(i) The typical width of the resonances can be much smaller than the optical pumping rate Γ' because of atom localization (Lamb-Dicke effect).

(ii) The intensity of overtones is generally much weaker than the intensity of Raman resonances. Their positions cannot always be simply deduced from the position of the Raman resonances. Conditions in which overtones can be observed have been found.

(iii) The shape of the central resonance is very sensitive to probe polarization. This central structure corresponds to a two-wave mixing resonance [24] and its shape and width give indications on the response times of the dynamical modes of the molasses that are excited by the probe.

(iv) The central resonance results from two contributions. The first is associated with the forward scattering of the pump copropagating with the probe on a global observable of the molasses. The second corresponds to the backward scattering of the counterpropagating pump on a spatially modulated grating. This second contribution gives indication on atom localization and on the existence of a large-scale spatial order.

All these points clearly show the importance of the localized bound states and of the periodic structure in this molasses configuration. An obvious prolongation of this work is to study the probe transmission in the case of a molasses obtained with two circularly cross-polarized trapping beams. In this case, the light shifts are space independent [6] and no bound states are expected for this configuration. Apart from Raman resonances between two differently light-shifted Zeeman sublevels [27] and two-wave mixing resonances having a width on the order of the optical pumping rate, one also expects to find here narrower Rayleigh resonances due to damping phenomena induced by the cooling friction force. The study of this molasses configuration will be the topic of a forthcoming paper.

Extension of this work to other cooling mechanisms can also be considered. For example, magnetic assisted Sisyphus cooling [28] also leads to a periodic modulation of the light shifts. Bound states may be obtained in such potentials and Raman transitions between different levels may be observed on a probe transmission spectrum. The case where cooling below the recoil limit is achieved [29] may also be interesting to consider.

We have considered in this paper only the probe transmission and the four-wave mixing generation because these are quantities that have been experimentally observed in our group [3,16]. Other possibilities such as the study of the fluorescence spectrum are also of interest and deserves some theoretical investigation. Even if one does not expect significant differences between the information that can be obtained from these various methods, there are, however, some subtle differences such as, for example, the occurrence of a purely elastic line in the fluorescence spectrum that should be studied.

Finally, even if it appears that the present study made for a $J_g=\frac{1}{2}\rightarrow J_e=\frac{3}{2}$ atomic transition is in satisfactory agreement with the experiments of [3] and [16] performed on a $J_g=4\rightarrow J_e=5$ atomic transition, one can wonder whether there are some interesting specific effects for a transition starting from a ground state having an angular momentum larger than $\frac{1}{2}$. For example, the fact that the eigenstates of the Hamiltonian associated with the light shifts are tensorial products of an internal state ($|g,-\rangle$ or $|g,+\rangle$) and an external state is something peculiar to a $J_g=\frac{1}{2}$ ground state. For $J_g>\frac{1}{2}$, this is no longer true and that may have some consequences on the line shapes. Another interest of this study would be of course to achieve a quantitative comparison between experiment and theory.

ACKNOWLEDGMENTS

We would like to thank C. Cohen-Tannoudji, Y. Castin, J. Dalibard, B. Lounis, C. Salomon, P. Verkerk, and P. R. Berman for many helpful discussions.

APPENDIX: COMMENTS ABOUT ATOMIC TRANSITIONS STARTING FROM A $J_g > \frac{1}{2}$ STATE

We want here to sketch some ideas about the way to derive probe transmission (or phase-conjugate reflection) spectra for $J_g\rightarrow J_e$ atomic transitions with $J_g>\frac{1}{2}$. The transmission spectrum of the probe beam depends on the mean value of operator $\wp_{\aleph}$ calculated from the modification of the density matrix $\sigma^{(1)}$. As in the case of a $J_g=\frac{1}{2}\rightarrow J_e=\frac{3}{2}$ transition, it is convenient to express this operator by means of quantities having a well-defined physical interpretation. One finds

$$\wp_{\parallel}=(\beta_0 I-2\beta_2\{\mathbf{J}\cdot\mathbf{e}_p\}^2)+(\beta_1 J_z+i\beta_2\{J_xJ_y+J_yJ_x\})e^{-2ikZ}\ , \tag{A1a}$$

$$\wp_{\perp}=(\beta_1 J_z+i\beta_2\{J_xJ_y+J_yJ_x\})+(\beta_0 I-2\beta_2\{\mathbf{J}\cdot\mathbf{e}_p\}^2)e^{-2ikZ}\ , \tag{A1b}$$

with

$$\beta_0=\frac{1}{\sqrt{6}}\frac{(2J_e+1)}{\sqrt{2J_g+1}}\begin{Bmatrix}1 & 1 & 0\\ J_g & J_g & J_e\end{Bmatrix}+\tfrac{1}{3}J_g(J_g+1)(2J_e+1)\times\left[\frac{15(2J_g-2)!}{(2J_g+3)!}\right]^{1/2}\begin{Bmatrix}1 & 1 & 2\\ J_g & J_g & J_e\end{Bmatrix}\ , \tag{A2a}$$

$$\beta_1=-\frac{\sqrt{3}}{2}\frac{(2J_e+1)}{\sqrt{J_g(J_g+1)(2J_g+1)}}\begin{Bmatrix}1 & 1 & 1\\ J_g & J_g & J_e\end{Bmatrix}\ , \tag{A2b}$$

$$\beta_2=(2J_e+1)\left[\frac{15(2J_g-2)!}{(2J_g+3)!}\right]^{1/2}\begin{Bmatrix}1 & 1 & 2\\ J_g & J_g & J_e\end{Bmatrix}\ , \tag{A2c}$$

where the quantities inside curly brackets are 6-J symbols. I is the identity operator which accounts for atomic density effects and J_z is the angular momentum along Oz,

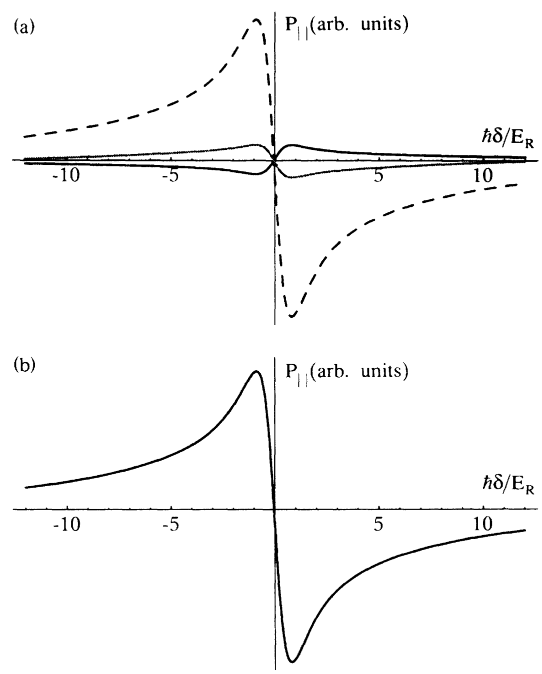

FIG. 12. Central resonance of the probe transmission spectrum in the $\aleph=\parallel$ polarization case for a $J_g=4\rightarrow J_e=5$ atomic transition. The spectrum was obtained by taking into account the first 40 band states with Bloch index $q=0,1$ for a detuning $\Delta=-10\Gamma$ and $\hbar|\Delta|s_0/E_R=1200$. (a) The contribution of the magnetization, the alignment and the index effects are, respectively, represented by a dashed, a solid, and a gray line. This figure clearly shows that both alignment and index effects are negligible in the case of deep optical potential wells. (b) The sum of these contributions gives a dispersionlike resonance in reasonable *quantitative* agreement with the experiment of [3].

which stands for polarization rotation due to magnetization gratings. In addition to these contributions, which were already present in the case of a $J_g=\frac{1}{2}\rightarrow J_e=\frac{3}{2}$ transition, one has to consider two additional contributions: $\{\mathbf{J}\cdot\mathbf{e}_p\}^2$ is the square of the angular momentum along the probe polarization which accounts for index effects on the propagation of the pump having the same polarization as the probe and $(J_xJ_y+J_yJ_x)$ corresponds to an alignment of the atomic medium and stands for the effects due to the probe-induced birefringence of the atomic sample. The terms depending on e^{-2ikZ} account for effects due to the backscattering of the pump wave which counterpropagates with the probe, whereas the terms independent on z represent contributions due to the copropagating pump beam.

One can wonder whether the additional contribution of the index effects and of the alignment leads to probe transmission spectra qualitatively different from those obtained in the case of a $J_g=\frac{1}{2}\rightarrow J_e=\frac{3}{2}$ transition. It is possible to estimate the order of magnitude of these contributions (which are both weighted by β_2) by comparison with the one of the orientation (weighted by β_1) through the calculation of the ratio β_1/β_2. The value of this ratio is reported in the following table:

	$J_g\rightarrow J_e=J_g-1$	$J_g\rightarrow J_e=J_g$	$J_g\rightarrow J_e=J_g+1$
β_1/β_2	$2J_g-1$	-1	$-(2J_g+3)$

which shows that the index and alignment effects become negligible compared to the orientation effects in the limit of large ground-state angular momenta both for a $J_g\rightarrow J_e=J_g-1$ and a $J_g\rightarrow J_e=J_g+1$ atomic transition, which is the case of the $J_g=4\rightarrow J_e=5$ transition of cesium used in [3]. Note, however, that in the case of small potential depths, the spatial extension of the wave functions will affect selectively the physical processes involving backscattering. For example, in the $\aleph=\|$ polarization configuration, the orientation contribution will be significantly lowered and become as important as the index and alignment contributions. In contrast, $J_g\rightarrow J_e=J_g$ atomic transitions for which all the contributions to (A1) have the same order of magnitude could lead to probe transmission spectra qualitatively different from those reported in this paper. We show in Fig. 12 the different contributions to the Rayleigh resonance of a probe transmission spectrum for a $J_g=4\rightarrow J_e=5$ transition in the $\aleph=\|$ polarization case. This spectrum is in reasonable *quantitative* agreement with the experimental observation of [3] and clearly shows that most of the signal is due to the orientation contribution which was the unique contribution in the case of a $J_g=\frac{1}{2}\rightarrow J_e=\frac{3}{2}$ atomic transition.

[1] Y. Castin and J. Dalibard, Europhys. Lett. **14**, 761 (1991).

[2] C. I. Westbrook, R. N. Watts, C. E. Tanner, S. L. Rolston, W. D. Phillips, P. D. Lett, and P. L. Gould, Phys. Rev. Lett. **65**, 33 (1990); see also N. P. Bigelow and M. G. Prentiss, *ibid.* **65**, 29 (1990).

[3] P. Verkerk, B. Lounis, C. Salomon, C. Cohen-Tannoudji, J.-Y. Courtois, and G. Grynberg, Phys. Rev. Lett. **68**, 3861 (1992).

[4] P. Martin, in *Many-Body Physics*, 1967, Les Houches Lectures, edited by C. de Witt and R. Balian (Gordon and Breach, New York, 1968); see also C. Cohen-Tannoudji, J. Dupont-Roc, and G. Grynberg, *Photons and Atoms* (Wiley, New York, 1989), p. 352.

[5] J. Guo, P. R. Berman, B. Dubetsky, and G. Grynberg, Phys. Rev. A **46**, 1426 (1992); J. Guo and P. R. Berman (unpublished).

[6] J. Dalibard and C. Cohen-Tannoudji, J. Opt. Soc. Am. B **6**, 2023 (1989).

[7] P. J. Ungar, D. S. Weiss, E. Riis, and S. Chu, J. Opt. Soc. Am. B **6**, 2058 (1989).

[8] C. Cohen-Tannoudji, in *Fundamental Systems in Quantum Optics*, Proceedings of the Les Houches Summer School of Theoretical Physics, Session LIII, edited by J. Dalibard, J. M. Raimond, and J. Zinn-Justin (Elsevier Science, Amsterdam, 1991).

[9] J. P. Barrat and C. Cohen-Tannoudji, J. Phys. (Paris) **22**, 329 (1961).

[10] Y. Castin, J. Dalibard, and C. Cohen-Tannoudji, in *Light Induced Kinetic Effects on Atoms, Ions, and Molecules*, edited by L. Moi, S. Gozzini, C. Gabbanini, E. Arimondo, and F. Strumia (ETS Editrice, Pisa, 1991), p. 363.

[11] W.-K. Tung, *Group Theory in Physics* (World Scientific, Singapore, 1985); N. W. Ashcroft and N. D. Mermin, *Solid State Physics* (HRW International editions, New York, 1976).

[12] D. Wineland and W. Itano, Phys. Rev. A **20**, 1521 (1979).

[13] Indeed, an experiment recently done at NIST shows that Rayleigh scattering is the dominant feature of the spontaneous emission spectrum [P. S. Jessen, C. Gerz, P. D. Lett, W. D. Phillips, S. L. Rolston, R. J. C. Spreeuw, and C. I. Westbrook, Phys. Rev. Lett. **69**, 49 (1992)].

[14] C. Cohen-Tannoudji, J. Dupont-Roc, and G. Grynberg, *Atom-Photon Interactions* (Wiley, New York, 1992), p. 328.

[15] For a review, see, for example, R. W. Boyd and G. Grynberg, in *Contemporary Non Linear Optics*, edited by G. Agrawal and R. W. Boyd (Addison-Wesley, Reading, MA, 1992).

[16] B. Lounis, P. Verkerk, C. Salomon, J.-Y. Courtois, and G. Grynberg (unpublished).

[17] C. Cohen-Tannoudji, J. Dupont-Roc, and G. Grynberg, in *Atom-Photon Interactions* (Ref. [14]), p. 384.

[18] A. Heidmann, thèse de 3^e cycle, Paris, 1984 (unpublished).

[19] J. Javanainen and S. Stenholm, Appl. Phys. **21**, 35 (1980).

[20] A. R. Bogdan, M. C. Downer, and N. Bloembergen, Opt. Lett. **6**, 348 (1981).

[21] G. Grynberg, M. Vallet, and M. Pinard, Phys. Rev. Lett. **65**, 701 (1990).

[22] M. Vallet, M. Pinard, and G. Grynberg, Opt. Commun. **87**, 340 (1992).

[23] D. S. Chemla, D. A. B. Miller, P. W. Smith, A. C. Gossard, and W. Wiegmann, IEEE J. Quantum Electron. **QE-20**, 265 (1984); see also C. Weisbuch and B. Vinter, *Quantum Semiconductor Devices: Physics and Applications* (Academic, New York, 1991).

[24] G. Grynberg, E. Le Bihan, and M. Pinard, J. Phys. (Paris) **47**, 1321 (1986).

[25] M. T. Gruneisen, K. R. MacDonald, and R. W. Boyd, J. Opt. Soc. Am. B **5**, 123 (1988).

[26] The interest in adiabatic states to help understand two-wave mixing resonances has been considered by G. Grynberg and P. Berman, Phys. Rev. A **39**, 4016 (1989) in the case of two-level atoms.

[27] D. Grison, B. Lounis, C. Salomon, J.-Y. Courtois, and G. Grynberg, Europhys. Lett. **15**, 149 (1991).

[28] B. Sheehy, S. Q. Chang, P. Van der Sraten, S. Hatamian, and H. Metcalf, Phys. Rev. Lett. **64**, 858 (1990).

[29] A. Aspect, E. Arimondo, R. Kaiser, N. Vansteenkiste, and C. Cohen-Tannoudji, J. Opt. Soc. Am. B **6**, 2112 (1989).

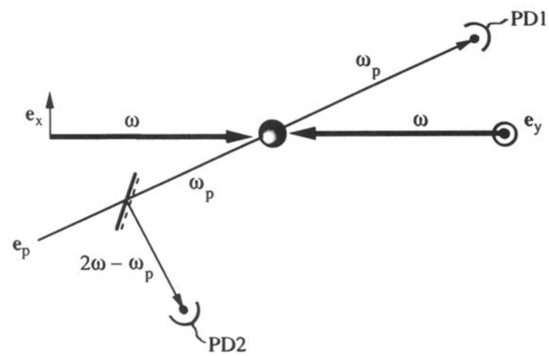

FIG. 2. Schematic experimental setup for pump-probe experiments. In addition to the cooling wave at frequency ω, a weak probe beam having linear polarization $\mathbf{e}_p$ and frequency ω_p is sent through the atomic medium (represented by a graduated sphere). By monitoring the probe intensity with photodiode PD1 as a function of the probe frequency, one has access to the probe transmission spectrum. The phase-conjugate reflected beam (frequency $2\omega-\omega_p$) can also be measured by means of photodiode PD2 (and of a plate located on the path followed by the probe beam).

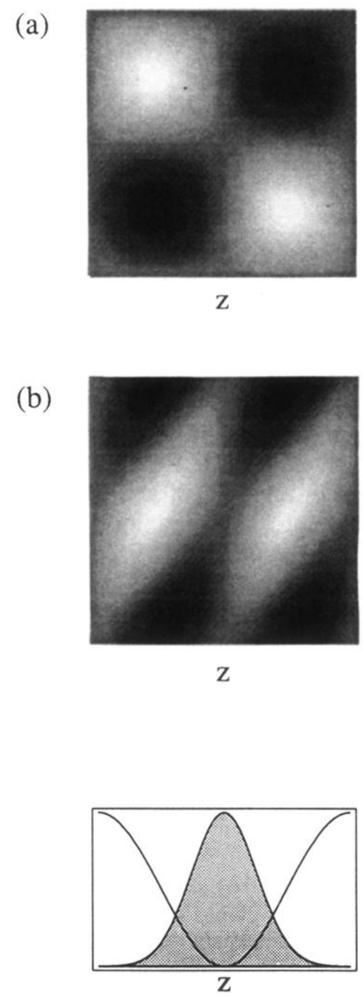

FIG. 8. Semiclassical representation of the probe-induced dissipative effects. The density plots represent the temporal evolution of $\pi_+^{(1)}(z)$. Black (white) color denotes a negative (positive) value of $\pi_+^{(1)}(z)$. It is possible to understand the effect of the probe by averaging $\pi_+^{(1)}(z)$ over the spatial extension of a band wave function (represented in gray at the bottom of the figure, for a single potential well). (a) $\aleph=\parallel$ polarization configuration. The average value of $\pi_+^{(1)}(z)$ for any band state is clearly equal to zero, so that the probe-induced dissipative effect does not lead to population changes. (b) $\aleph=\perp$ polarization configuration. The average value of $\pi_+^{(1)}(z)$ for any band state is nonzero and oscillates in time. The probe-induced dissipative effect thus leads to alternative population transfers from one potential well to the other. It is interesting to note that the value of $\pi_+^{(1)}(z)$ for $z=0$ is constant equal to zero, which means that an infinitely localized atom would not be affected (in the semiclassical limit) by the dissipative effects due to the probe. We have checked that the population of the lowest vibrational levels are less affected than the others for sufficiently deep potential wells.

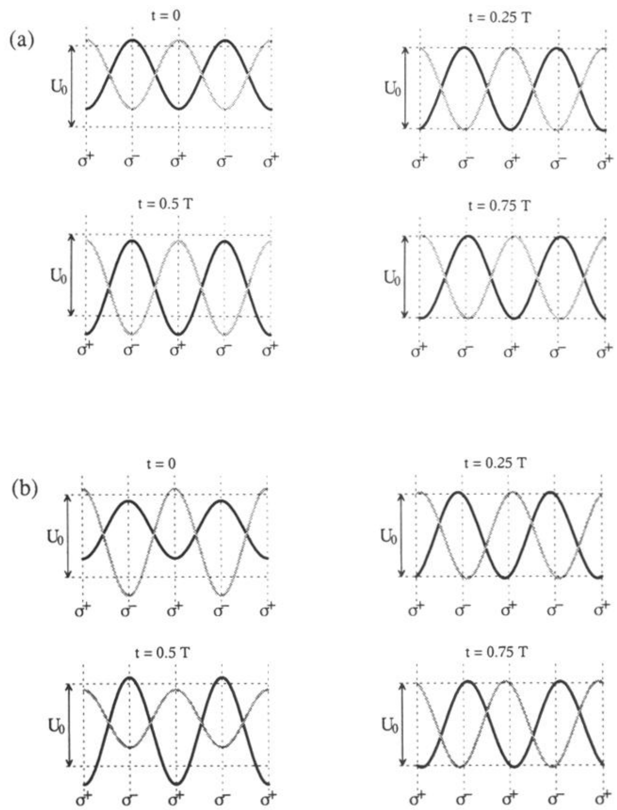

FIG. 9. Probe-induced modifications of the optical potential. The dashed lines permit us to localize the potential wells in absence of probe. The black (gray) potential corresponds to the $|g,+\rangle$ ($|g,-\rangle$) ground-state Zeeman sublevel. The local polarization of the cooling wave is indicated. We have represented the potential shapes at four different times during a period $T=2\pi/|\omega-\omega_p|$. At $t=0$ and 0.5 T the potential depth is modified, whereas at $t=0.25$ and 0.75 T the potential wells are translated in space. These potential changes lead to population modifications due to the tendency of the cooling beams to adapt the population distribution to the new potential shape. (a) $\aleph=\|$ polarization configuration. The potential wells associated with the two Zeeman sublevels are simultaneously modified so that the population changes are the same in each potential well. (b) $\aleph=\perp$ polarization configuration. The potential wells associated with the two Zeeman sublevels are modified with a phase delay of π, so that the population changes are opposite in adjacent potential wells.